

Robert Schwarzl, BSc

Femtosecond Transient Absorption Microscopy of Textured Anilino Squaraine Thin Films to Investigate Population Dynamics of Davydov States

MASTER'S THESIS

to achieve the university degree of
Diplom-Ingenieur

Master's degree programme: Technical Physics

submitted to

Graz University of Technology

Supervisor

Assoc.Prof. Markus Koch, Dipl.Ing. Dr.techn.
Institute of Experimental Physics

Graz, October 2021

AFFIDAVIT

I declare that I have authored this thesis independently, that I have not used other than the declared sources/resources, and that I have explicitly indicated all material which has been quoted either literally or by content from the sources used. The text document uploaded to TUGRAZonline is identical to the present master's thesis.

Date, Signature

Contents

1. Introduction	13
1.1. Transient Absorption Microscopy (TAM)	13
1.2. Measured units	14
1.3. Processes in transient absorption	14
1.4. Light sources	15
2. Devices and Setup	17
2.1. Characterisation	17
2.1.1. Spatial resolution	17
2.1.2. Temporal resolution	19
2.1.3. Accuracy	20
2.2. Chopper	20
2.3. History of the setup	26
2.3.1. Polarisation	26
2.3.2. Detection	27
2.4. Spectra of the NOPAs	27
2.5. Spatially separated pump-probe (SSPP)	29
3. Methods	33
3.1. Transient absorption (TA)	33
3.2. Scan modes	34
3.3. Microscopy and scaling	35
3.4. Spatial overlap and point spread function	37
3.5. Fit model for state population	38
4. Samples	41
4.1. Molecular crystals	41
4.1.1. Davydov splitting	41
4.2. Squaraines and SQIB	42
4.2.1. Sample degradation due to photodamage	46
5. Results	49
5.1. Excited states: Zero-crossing points into excited state absorption	50
5.1.1. 730 nm probe: Oscillations	56
5.2. Femtosecond Dynamics	58
5.2.1. Population transfer	58
5.2.2. Polarisation scan at 450 nm probe	59
5.3. Transient Absorption Imaging	63

5.4. Linear delay scan series	71
6. Outlook	73
6.1. Ultrafast exciton dynamics	73
6.2. Oscillations	73
6.3. Setup	73
A. List of Devices	75
B. List of Figures	77
C. List of Tables	79

Abstract

SQIB, an abbreviation for squaraine with iso-butyl side chains, is an anilino squaraine that forms molecular crystals after deposition and annihilation on a glass surface. A specific, orthorhombic modification is of particular interest as its texture consists of domains of diameters from 10 μm to 200 μm with uniform orientation called *platelets*. These show a very large Davydov splitting with an energy difference exceeding 0.2 eV. Also, the projected transition dipole moments into these split excitations are arranged perpendicularly, allowing for a selection of specific transitions not only by choice of wavelengths, but also by varying the linear polarisation of incident light. The microstructured nature of orthorhombic SQIB samples makes the use of transient absorption microscopy particularly useful as it opens up the possibility of performing spectroscopic analysis of single domains with femtosecond time resolution, micrometer spatial resolution and almost six orders of magnitude of sensitivity on light intensity changes.

Measurements indicate the existence of higher excited states where single excitations show lifetimes below 10 ps which can only be investigated using femtosecond lasers, partly due to the high susceptibility of the material against photo damage, forbidding the use of high-powered CW sources for multi-photon experiments. These higher excited states show a similar Davydov splitting as the first excitations, resulting in polarisation dependencies. These also show that excited states can, to an extent, be selectively excited by using different linear input polarisations as described in the literature on squaraines. Another effect discovered during delay scan measurements is an oscillating behaviour in transient absorbance in delay scan measurements when probing the lower Davydov band. Comparison to literature suggests coherent phonon oscillation as source of this phenomenon. Additionally, femtosecond dynamics of the material are investigated by applying a model of multiple exponential decays to the delay scans. While these are still under investigation, there are indications for very fast population transfer from the upper into the lower Davydov band shown by stimulated emission, followed by non-radiative decay prevailing as ground state depletion. Finally, the capabilities of the transient absorption microscope to create images are shown, showcasing the transient behaviour for large areas of the sample. Boundaries between different platelets are of particular interest here.

A large part of the work for this thesis is associated with finalising and commissioning the ultrafast transient absorption microscopy setup (UTAM), as well as the establishment of new measurement methods. Examples are the introduction of a mechanical chopper to improve the signal-to-noise ratio as well as measurement times significantly, and the discovery of characterisation of sample degradation as part of SQIB results. Measurement modes include delay scan series at different points, transient absorption imaging and polarisation scans.

Kurzfassung

SQIB, eine Abkürzung für Squarain mit Isobutyl-Seitenketten, ist ein Anilino-Squarain, das nach Abscheiden und Tempern auf einer Glasoberfläche Molekulkristalle ausbildet. Eine bestimmte orthorhombische Modifikation ist besonders interessant, da sich darin Domänen mit Durchmessern von 10 μm bis 200 μm ausbilden, welche auch *Platelets* genannt werden. Diese Platelets haben ein besonders großes Davydov splitting mit einer Energiedifferenz über 0.2 eV. Weiters stehen die transienten Dipolmomente der beiden Exzitonen genau normal aufeinander, was eine selektive Anregung der Zustände nicht nur über eine geeignete Wahl der Wellenlänge, sondern auch über eine gerichtete lineare Polarisierung erlaubt. Die Nutzung eines Transiente-Absorptions-Mikroskops zeigt an diesen Proben ihre besondere Stärke, da sie spektroskopische Untersuchungen mit Femtosekunden-Zeitauflösung, Mikrometer-Ortsauflösung und einer Empfindlichkeit auf Intensitätsänderungen von fast sechs Größenordnungen ermöglicht.

Messungen deuten die Existenz höher angeregter Zustände mit Lebensdauern unter 10 fs an, die nur mit Femtosekundenlasern untersucht werden können. Dies liegt insbesondere an der Empfindlichkeit des Materials gegenüber Lichtschäden an, was kontinuierliche Strahlquellen für Mehrphotonenspektroskopie verunmöglicht. Diese höher angeregten Zustände zeigen ein ähnliches Davydov splitting wie die niedriger angeregten Zustände, was sich durch die Polarisationsabhängigkeit zeigt. Damit wird auch bewiesen, dass eine selektive Anregung zum Teil durch die Wahl der linearen Polarisationsrichtung gelingt. Ein weiterer Effekt zeigt sich in oszillierendem Verhalten der transienten Absorbanz bei Einstellung des Probe-Lasers auf das lower Davydov band. Vergleiche mit der Literatur legen nahe, dass dieses Phänomen auf kohärente Phononenooszillationen zurückzuführen ist. Weiters wird eine Untersuchung von Femtosekunden-Dynamiken mithilfe eines Modells mehrerer exponentieller Zerfälle vorgenommen. Als vorläufige Resultate zeigen diese Messungen einen Populationstransfer in das lower Davydov band durch die Existenz von stimulierter Emission bei dessen Probe-Wellenlänge, anschließend durch einen nicht-radiativen Zerfallspfad, der mit reinem ground state depletion einhergeht. Zuguterletzt werden die Fähigkeiten des Transiente-Absorptions-Mikroskops gezeigt, die Dynamiken großer Flächen auf der Probe als Bild darzustellen. Grenzen zwischen verschiedenen Platelets sind hier von besonderem Interesse.

Große Teile der Masterarbeit bestehen aus Finalisierung und Inbetriebnahme des ultraschnellen Transiente-Absorptions-Mikroskops (UTAM) und der Einführung neuer Messmethoden. Dazu gehören das Einbringen eines mechanischen Choppers zur Verbesserung von Rauschverhältnis und Messzeit und die Charakterisierung der Schädigung von Squarain-Proben nach langen Messzeiten. Einige der Messmethoden sind Delay-Scan-Messungen an verschiedenen Punkten, Transiente-Absorptions-Bildgebung und Polarisationsscans.

Acknowledgements

Work for this master thesis was conducted in the research group of Markus Koch at the Institute for Experimental Physics at the University of Technology, Graz (TU Graz). In spite of limitations risen by the COVID-19 pandemic, the institute made great efforts to sustain active, experimental research, be it by Bachelor, Master and PhD students up all the way to professors. I am very grateful to Markus Koch, the institute head Martin Schultze and the members of our group, Pascal Heim, Leonhard Treiber, Michael Stadlhofer, Kerstin Absenger, Bernhard Thaler, Leo Felix Angermann, as well as other people involved in making the best of this gruesome situation. Also, I want to emphasise the amount of effort that is put into careful supervision and frequent discussions in this group by Markus Koch and all other members which greatly helped with working in such an interesting, novel field of physics.

As work on femtosecond dynamics can not be done by oneself, I particularly want to thank Pascal Heim as my primary contact for every aspect associated with femtosecond theory and experiments and partner on the transient absorption microscope. Furthermore, I want to thank Manuela Schiek as a cooperating partner for providing all of the samples and for critical discussions of the preliminary results. During the course of working for this thesis, I had the pleasure to be introduced to the work of Dario Grimaldi and Joachim Krenn's group at University of Graz on the transient absorption microscope as well as to explain its working principles to Leo Felix Angermann. I wish Dario and Leo best of luck in their further work.

Last but not least, it would not have been possible for me to actively pursue my course of studies up to this thesis without the moral and financial support of my parents Annemarie Schwarzl-Troyer and Ernst Schwarzl. Thank you for allowing me to achieve this milestone.

1. Introduction

1.1. Transient Absorption Microscopy (TAM)

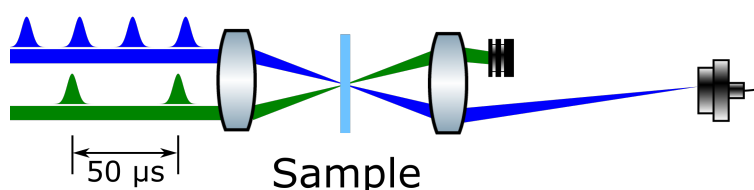


Figure 1.1.: Principle of transient absorption microscopy. The variation in intensity in the blue probe laser pulses due to the interaction of the green pump pulses with the sample is measured using the photodiode to the right. Optical components by reference [5].

Transient absorption is a technique where two laser pulses called *pump* and *probe* interact with a sample within a specified time delay between them. After the pump beam photo-excites the sample, the change in intensity in the probe pulse is analysed using a photodiode.

By focussing both pump and probe beam towards a common spot on a sample, as shown in figure 1.1, spatial resolutions close to the diffraction limit can be obtained. Techniques such as saturated transient absorption allow resolutions down to 100 nm (see reference [12]) by spatially modulating the pump excitation field. The ability to have focus sizes on the nanoscale also opens up the possibility of studying for example the carrier transport in nanowires [6] and perovskites [8], improving the understanding of processes in organic solar cells. A good overview over various other application and proposed or implemented improvements is given in references [3] and [17].

In this thesis, a transient absorption microscope is used to investigate excited states and femtosecond dynamics inside the orthorhombic molecular crystal modification of anilino squaraine with isobutyl side chains (SQIB). The setup offers down to $3 \mu\text{m}$ of spatial resolution, less than 100 fs of temporal resolution and a signal-to-noise ratio of 5×10^{-6} OD (almost six orders of magnitude).

1.2. Measured units

In transient absorption, the most important value recorded is the ratio between the probe intensity with a pump pulse and without this pump pulse:

$$\Delta T = \frac{I_{\text{probe}} + \Delta I_{\text{pump,probe}}}{I_{\text{probe}}} = 1 + \frac{I_{\text{pump,probe}}}{I_{\text{probe}}} \quad (1.1)$$

We hereby define I_{probe} as the probe-only intensity and $\Delta I_{\text{pump-probe}}$ as the difference introduced by the interaction of the pump pulse with the sample. ΔT is often given in %, I can be voltages (V) or powers (W). To better indicate the absorbing behaviour of the material under investigation, the transient change in absorbance is calculated from this value:

$$\begin{aligned} \Delta A &= -1000 * \log_{10}(\Delta T) \\ &= -1000 * \log_{10} \left(\frac{\Delta I_{\text{pump,probe}} + I_{\text{probe}}}{I_{\text{probe}}} \right) \end{aligned} \quad (1.2)$$

Due to the logarithmic scale, the resulting values are given in orders of magnitude (ΔOD), most often in ΔmOD . The transient absorbance decreases when the material becomes more transparent for the probe pulse after excitation and increases when it becomes more opaque.

What is actually measured using the photodiode shown in Figure 1.1 is a signal with alternating peaks. Assuming that even peaks include the pump excitation whereas odd peaks do not, the signal at the oscilloscope consists of:

$$V_{\text{total}}(t) \propto (\Delta V_{\text{pump,probe}}(t) + V_{\text{probe}}(t) + V_{\text{background}}(t)) \quad (1.3)$$

$\Delta V_{\text{pump-probe}}$ and V_{probe} are extracted by Fourier transforming the signal as described in reference [10]. This can be done due to the periodic nature of the laser pulse being emitted. As long as there is no external light source at the laser repetition rate or its whole fractions (harmonics of a non-sinusoidal signal), and the total signal is within the set limits of the oscilloscope, the signal can be extracted reliably.

1.3. Processes in transient absorption

Excitations in the material result in various processes that change the intensity of the probe beam. As also described in figure 1.2, processes likely involved in the results achieved in this thesis are:

- Ground state depletion (*GSD*) or ground state bleach (*GSB*): The pump beam decreases the population in the ground state via excitation into a state that is not sensitive to the probed transition. This reduces the density of filled states available for interaction with the probe beam and leads to a more transparent sample resulting in a negative ΔA signal.

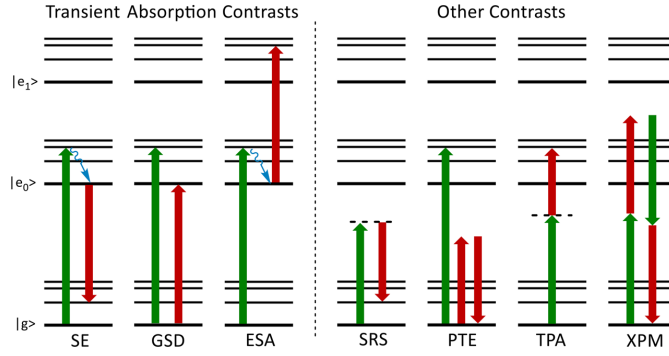


Figure 1.2.: Contrast mechanisms in transient absorption. SE: stimulated emission, GSD: ground state depletion (also called ground state bleach in this thesis), ESA: excited state absorption are all related to excited state information whereas SRS: stimulated raman emission, PTE: photothermal effect, TPA: two photon absorption and XPM: cross phase modulation do not. Source of image and explanation: reference [17], cropped

- Excited state absorption (*ESA*): Especially in cases where the band structure allows further excitation of states that were previously excited by the pump beam, an increase of opacity for the probe beam can be observed resulting in positive ΔA signals.
- Stimulated emission (*SE*): In case of a matching energy between a transition with population in its upper state and an incoming photon, another photon may be emitted. As this leads to an increase in intensity after interaction with the sample, SE shows as an increase in transparency and a negative ΔA signal.

GSD and SE can, in principle, be distinguished by the difference in lifetime. While GSD is expected to be the slowest process as all of the excited states need to decay back to their ground state, SE shows no such lower limit. Furthermore, delay scans often show a superposition of different effects. One example can be found in section 5.1.1.

As indicated in reference [17] and figure 1.2 there are several other processes contributing to the total contrast in transient absorption. However, these do not provide insight into excited states of the material. Examples include the spikes of varying transient absorbance often appearing close to the temporal overlap in delay scans which could be attributed to cross-phase modulation.

1.4. Light sources

To achieve femtosecond resolution, a commercial mode-locked Yb:KGW laser (Light Conversion PHAROS) is used to pump two non-collinear optical parametrical amplifiers (NOPAs, Light Conversion Orpheus-N). These use white light generation (WLG) to achieve a broad spectrum of colours within a chirped pulse. Second and third harmonics

generation (SHG, THG) are used to achieve suitable photon energies for parametrical amplification in a series of two non-linear crystals. As a result, the operator of the setup can tune both laser wavelengths separately and achieve less than 100 fs of temporal resolution throughout the available spectrum. The setup is explained in more detail in chapter 2.

In order to maximise signal-to-noise ratio, the laser sources are paired with a mechanical chopper capable of blocking every second pulse, effectively allowing shot-to-shot measurements. Compared to measurements without the chopper, this facilitates an enormous increase in signal-to-noise ratio per measurement time of more than 10000, largely due to source instabilities. It should be noted that due to the sensitivity of SQIB samples against long exposure to laser radiation, the measurements in this thesis would likely not have been possible without the introduction of shot-to-shot comparisons.

The squaraine samples investigated in this thesis are oriented in the same (or, at least, similar) directions only on relatively small platelets ranging from a few μm up to hundreds of μm . This necessitates the use of a transient absorption microscope to focus both beams and bring them to alignment (*spatial overlap*) on the sample's surface. According to calibration measurements, the setup at TU Graz can reach a beam width of below $4\mu\text{m}$ and pulse durations at or below 80 fs depending on the wavelength, making this instrument very capable for the purposes of investigating the exciton dynamics of squaraines.

2. Devices and Setup

As can be seen in figure 2.1, the transient absorption microscope is set up the following way:

1. Pharos output power of 16 W at 40 kHz repetition rate and 1030 nm of central wavelength, resulting in 400 μ J per pulse, is split 50:50 between the non-collinear optical parametric amplifiers ORPHEUS-N-3H (500 nm to 950 nm) and ORPHEUS-N-2H (650 nm to 950 nm).
2. The pump beam is focused through a chopper, discarding every second pulse, using $f = 125$ mm plano-convex lenses.
3. The probe beam or the pump beam is delayed using a delay stage. Considering the total range of the delay stage, 5 cm, a factor of 2 corresponding to the double propagation of the beam and the speed of light, a total delay range of 334 ps can be utilised:

$$\Delta t = 2 * \frac{\Delta s}{c} \approx 2 * \frac{5 \times 10^{-2} \text{ m}}{299\,792\,458 \text{ m s}^{-1}} \approx 334 \text{ ps} \quad (2.1)$$

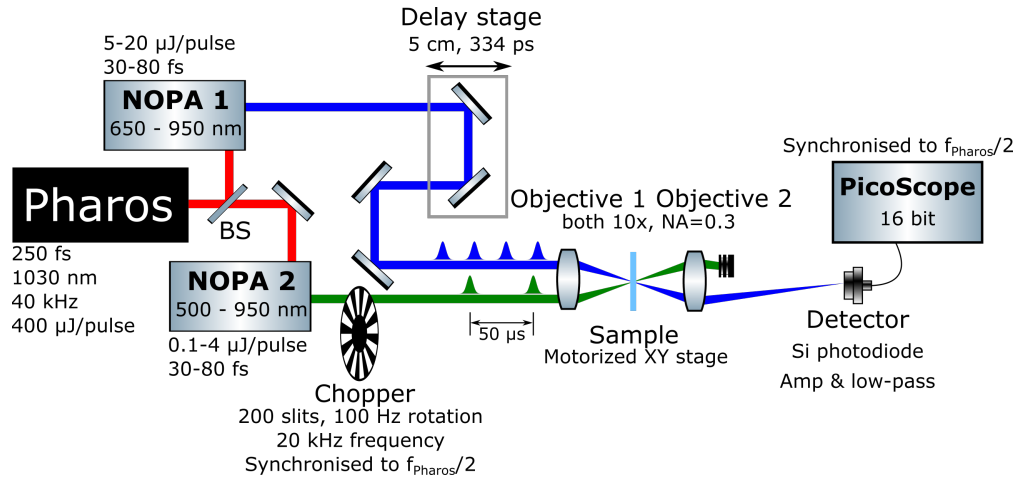
with Δt : total delay range, Δs : movement range, c : speed of light. Which delayed path is chosen depends on the wavelength requirements, i.e. if the extended range of the Orpheus N-3H down to 500 nm is needed for pumping or probing.

4. Both beams pass through multiple OD filters (reflective and absorptive) to set the correct output power.
5. The polarization is adjusted as close as possible to the entrance objective to prevent unwanted changes in reflectivity. For this, achromatic $\frac{\lambda}{2}$ plates are used.
6. Both beams enter the first objective in parallel. They are refracted in a way that they exactly overlap within the sample.
7. Depending on the wavelengths selected, the pump beam can either be filtered using edge pass filters (e.g. a FELH0700 long pass) or by dumping the pump beam mechanically. This is done at varying positions between the imaging objective and the detector.

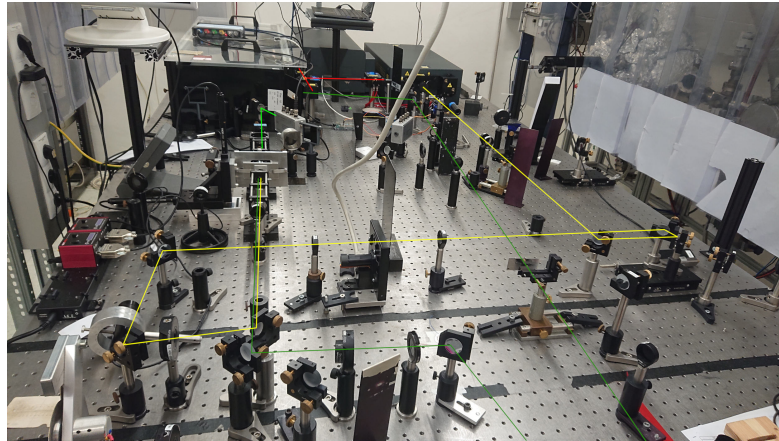
2.1. Characterisation

2.1.1. Spatial resolution

To determine the maximum spatial resolution of the microscope, reference [10] used a cross consisting of thin-film gold bars on a glass surface and scanned the laser spot over



(a) Sketch of the transient absorption microscope including properties relevant for experiments. Provided by reference [10], optical components by reference [5], modified.



(b) Image of the transient absorption microscope. Red indicates the Pharos pump beam, yellow the Orpheus-2H beam used as pump and green the Orpheus-3H beam used as probe.

Figure 2.1.: Setup of the transient absorption microscope. Figure 2.1b also shows absorptive and reflective neutral density filters, lenses for focussing through the chopper and $\frac{\lambda}{2}$ plates for polarisation setup.

it. Assuming a close to instant (nm) slope of the edge of the gold bar and a Gaussian point spread function:

$$\sigma_{\text{Au}} \ll \sigma_{\text{Laser}} \rightarrow T_{\text{Au}}(x) \approx \Theta(x)$$

σ : standard deviation ($[x] = [\sigma] = 1 \mu\text{m}$), $T_{\text{Au}}(x)$: transmission on the edge of a gold bar, $\Theta(x)$: Heaviside function ($[T] = [\Theta] = 1$), the resulting convolution is a Gaussian cumulative distribution function:

$$\int_{-\infty}^{\infty} \Theta(x_0 - x) \frac{I(x)}{Z} dx = \frac{1}{Z} \int_{x_0}^{\infty} I(x) dx = 1 - \frac{1}{Z} \int_{-\infty}^{x_0} I(x) dx \quad (2.2)$$

assuming an intensity distribution $I(x)$ with a normalised power of Z in one dimension and using the symmetry of a Gaussian distribution for the last step. Using **Matlab**'s **nlinfit** for fitting and **erfc** (complementary error function), the standard deviation can be fitted as a measure of spatial resolution:

$$\sigma_x = 4.51 \mu\text{m} \quad (2.3)$$

$$\sigma_y = 2.87 \mu\text{m} \quad (2.4)$$

with uncertainties well below the variation between different measurements; this indicates about $3 \mu\text{m}$ of vertical resolution and $5 \mu\text{m}$ of horizontal resolution at minimum spot size, actual numbers vary with the degree of optimisation, especially the aperture of irises and position of focussing lenses, done before a measurement and could be even lower. Figure 2.2 shows the corresponding images. See also the Matlab documentation of **normpdf**¹ for the relation between normal distributions and the complementary error function.

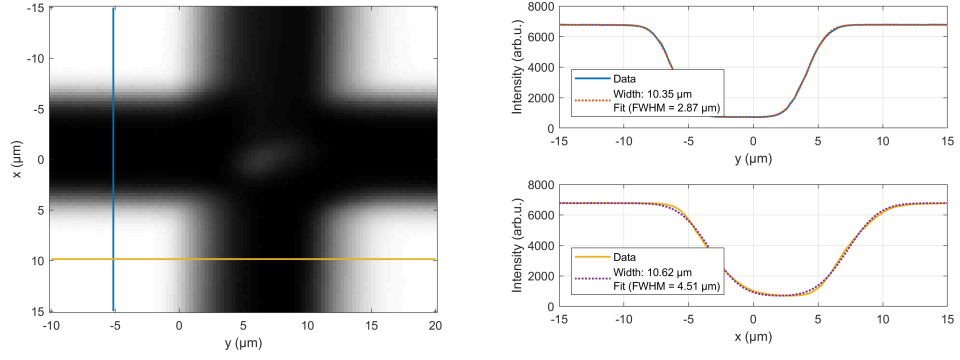
For comparison, the first objective is optimised to achieve minimum spot size on the camera which is placed instead of a sample. This can be done until there is only one pixel in full illumination, resulting in less than $3.75 \mu\text{m}$ in beam diameter (pixel size of the camera used). Directly neighbouring pixels only have $\approx \frac{1}{5}$ of the intensity in the central pixel which is in saturation.

2.1.2. Temporal resolution

To determine the temporal resolution of the setup, both pump and probe beam are set to the same wavelength and focused onto a 1 mm β -Barium Borate (BBO) SHG crystal. Then, the delay is adjusted to achieve a cross-correlation spot behind the crystal in between of the single-pulse SHG spots. After selecting this spot with an iris, it is focussed onto the detector using a concave mirror. By scanning the delay stage over the total range of this spot appearing, the cross-correlation of the envelope of both beams can be measured. Assuming a Gaussian pulse shape, their standard deviations follow the relationship $\sigma_{\text{pump}}^2 + \sigma_{\text{probe}}^2 = \sigma_{\text{cc}}^2$. One of the actual measurements taken after optimising both NOPAs at 700 nm with a total of $\approx 80 \text{ fs}$ can be seen in figure 2.3.

The temporal resolution can be improved iteratively by adjusting the prism compressors in both NOPAs using the **Prism insertion** and **Compressor length** settings

¹<https://www.mathworks.com/help/stats/normcdf.html>



(a) Image produced by measuring intensity while scanning the laser pulse over a gold cross on glass. (b) Error function fit on the cross-sections indicated. Width: Total width of the gold bar, FWHM: Full width half maximum of the slope.

Figure 2.2.: Determination of the resolution limit of the TAM setup.

in WinTopas. While the NOPAs are delivered with settings optimised for short pulse durations, the integrated prism compressor can also be used to compensate for linear chirp introduced later in the setup. This is caused by optical elements the beam paths pass through like lenses, neutral density filters, waveplates and polarisers. Beginning with default settings at each wavelength, it is recommended to scan each value in steps of 2000, measuring the cross-correlation scan for each new setting to determine the influence on pulse duration.

2.1.3. Accuracy

To determine the accuracy of points within a TA measurement, one can subtract the entire signal using equation (3.11) and calculate the standard deviation of the remaining background absorbance. For a series of 10 measurements, this yielded the result

$$\sigma(A) = 38 \mu\text{OD}$$

for a series of 10 specific measurements at standard conditions which is well within the observed range of 50 μOD in other measurements.

2.2. Chopper

At the beginning of the work on this master thesis, pump and probe beams were already set up to achieve transient absorption on the sample. For separate measurements, pump and probe beams could be blocked separately with anodised aluminium plates operated by servos. While this method is suitable for producing TA time scans, the inherent limitations in speed lead to the need for long integration times (often > 10 s per measurement point) as well as good blocking of background light. Accuracy is also limited

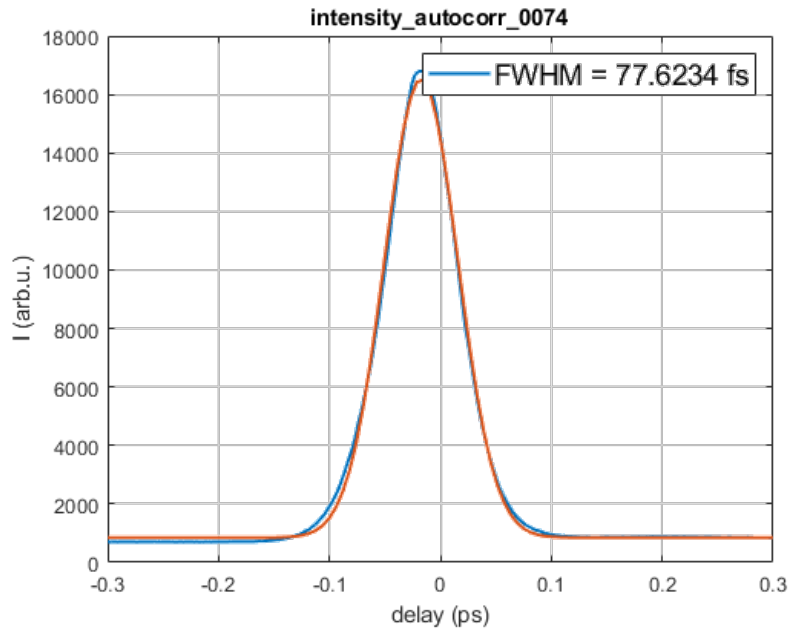


Figure 2.3.: Cross-correlation measurement for determining the temporal resolution at the sample at 700 nm. Both beams were focussed into a 1 mm β -Barium Borate crystal for SHG generation. The blue curve shows the cross-correlation intensity over pump-probe delay; the orange curve is a Gaussian fit from which the FWHM value is calculated.

by fluctuations in output power originating from the non-collinear optical parametrical amplifiers.

For this reason, an optical chopper was introduced into the pump beam. Combined with two $f = 125$ mm plano-convex, spherical N-BK7 lenses to narrow down the focus into less than the slit width of the chopper, true shot-to-shot measurements can be achieved at the maximum repetition rate of 40 kHz. The focal width of the lenses was chosen for spacing to the chopper and other optical elements.

Acoustic noise

The chopper used, a SciTec 310CD high speed chopper, caused concerns over the amount of vibration introduced into the laser setup. For this reason, it was mounted to a second optical table outside the final setup using a wooden stand with screws. Then, the app Spectroid ² was used on a Sony Xperia XZ2 Compact smartphone to measure the sound spectrum. A 5 V TTL signal from a function generator was fed into the chopper synchroniser which regulates frequency and phase of the chopper to the input signal.

Results from the sound measurements can be seen in figure 2.4. Compared to the background spectrum, a 10 kHz chopping frequency results in a noticeable increase in noise around 1000 Hz while the rotation frequency is overshadowed by the background. Beginning with 20 kHz, the rotation frequency becomes clearly visible at 100 Hz, 200 Hz and 278 Hz. Generally, these results indicate that the chopper, up to its mainly used speed of 20 kHz, does not increase sound levels so much as to influence the laser optics on the optical table and in the NOPAs themselves. It should, however, be avoided to run the chopper at its maximum speed due to the possible influence on power jitter.

Using a Coherent LabMax Pro pulse measuring head, the influence of chopper operation on energy variation was determined. Within the margin of uncertainty, there was no change for 20 kHz of chopping frequency whereas $\frac{\sigma}{\mu}$ (standard deviation divided by mean energy of a laser pulse train) increased by ≈ 1 % at 40 kHz, compared to $\approx 4.5(5)$ % originally.

For the final assembly of the chopper, a steel plate is manufactured with M3 bores and 3.5 mm mounting holes (corresponding to the positions on the 310CD case) as well as 6.5 mm holes for mounting to the optical table. However, for more flexibility, the steel plate is mounted to the table using post mounting brackets with aluminium or wooden spacers. At 20 kHz of chopping frequency, no influence can be measured on $\frac{\sigma}{\mu}$ (output power jitter). Introduction of shot-to-shot measurements into the setup improves measurement times from several hours for a TA delay scan to several minutes, depending on delay resolution and signal-to-noise ratio needed for a specific measurement. Apart from time constraints, this also allows for sensitive samples to be scanned reliably as spot degradation can become noticeable very quickly.

²<https://play.google.com/store/apps/details?id=org.intoorbit.spectrum>

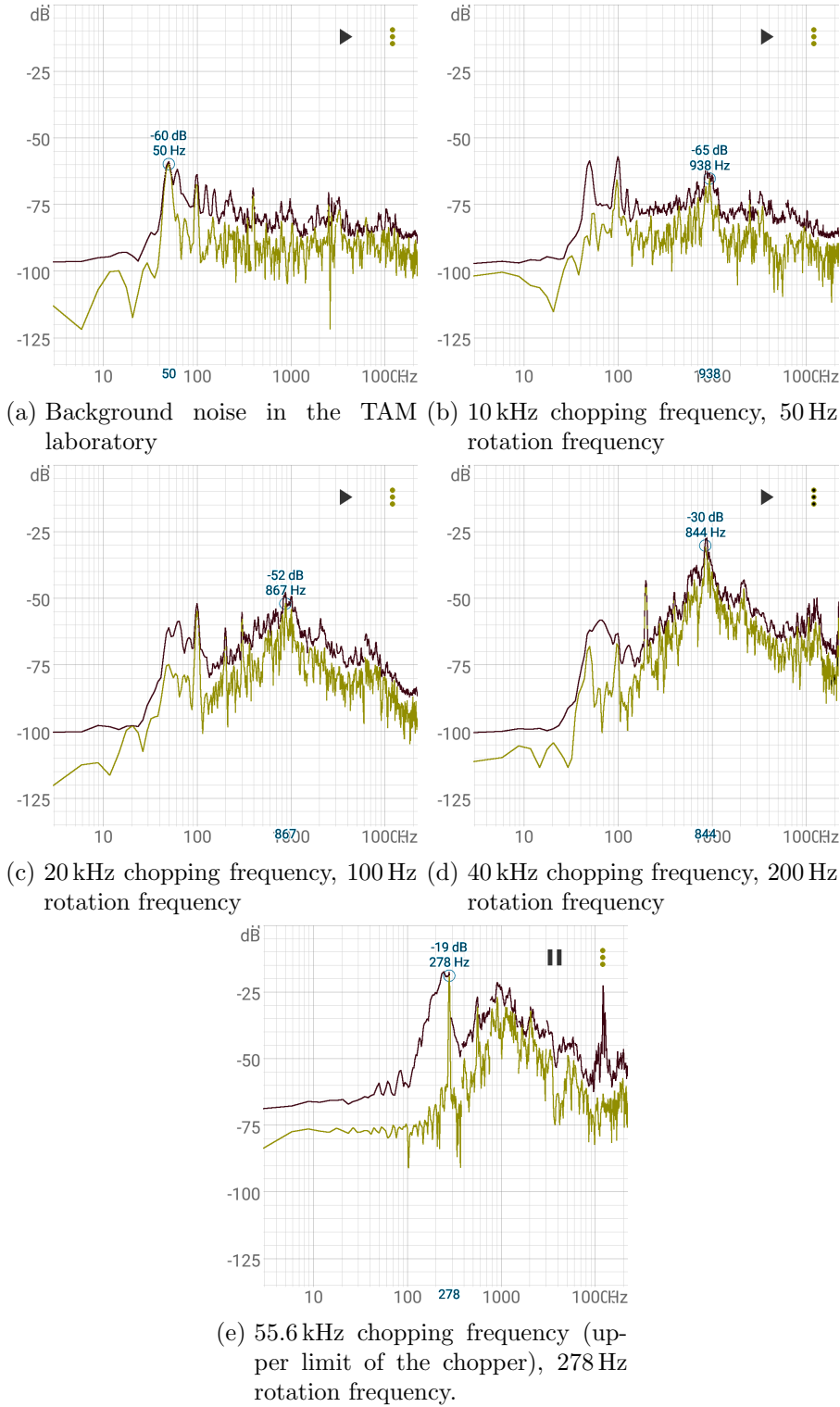


Figure 2.4.: Sound spectra of the chopper recorded with a smartphone running Spectroid from ≈ 1 m distance. Red: Maximum volume. Yellow: Current volume.

Synchronisation

Apart from the chopper controller and the chopping head itself, a synchronisation device is used to phase-lock the chopper to the laser clock signal. Before introducing the chopper to the main setup, the synchroniser is tested using a laser diode, focussing lenses and a photodiode. The goal is to determine the phase difference between photodiode and input signal as well as the amount of phase jitter (i.e. how much the phase varies with time):

$$\Delta\phi = \phi_{\text{chopper}} - \phi_{\text{reference}} \quad (2.5)$$

assuming periodic square waves for both signals. We define the peak-to-peak variation in $\Delta\phi$ as *phase jitter*; it is of particular importance for the shot-to-shot measurements as blocking at 20 kHz has to work reliably for the finite focus size achievable with 125 mm lenses, a suitable choice constrained by the dimensions of the chopper head itself. Figure 2.5 illustrates the simple measurement setup.

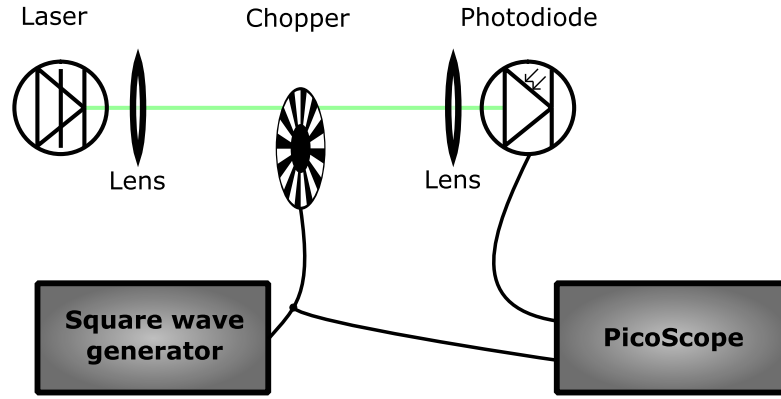


Figure 2.5.: Setup for the calibration of the chopper synchroniser. Laser: Thorlabs PL203 laser pointer, lenses: 125 mm plano-convex Eksma N-BK7 with focus inside the chopper wheel, chopper: SciTec 310CD with 200 slits and synchroniser, photodiode: Hamamatsu S1223 (without amplifier, but negatively biased at 4.5 V).

The lenses are adjusted to achieve minimum focus size at the chopper wheel, resulting in maximum edge steepness in the resulting signal from the photodiode. Assuming square wave signals, the phase difference can be determined by subtracting the points in time of rising or falling edges. These can be determined using the following algorithm:

1. Using indices $i \in \mathbb{N}$ and voltages U_i : Calculate moving mean μ_i from 100 samples of $U_{i,\text{photodiode}}$ each (at 5 kHz: 500 samples) and define a threshold $U_{\text{thresh}} := \max_i U_i - \min_i U_i$
2. Find rising edge indices $j \subset i$ where $\mu_j > U_{\text{thresh}} \wedge \mu_{j-1} < U_{\text{thresh}}$
3. Calculate difference between times $t_{j,\text{photodiode}} - t_{j,\text{reference}}$

4. Divide by average period in photodiode $\langle t_{i,\text{photodiode}} - t_{i-1,\text{photodiode}} \rangle$ between rising edges

Calculating this results in a graph of the phase difference relative to the total period. Using a sampling rate of $62\,500\text{ s}^{-1}$ and a bit depth of 16 bit, figure 2.6 shows multiple results at different chopping frequencies. Note that the maximum deviation of 25.7 % still allows for $\approx 50\%$ of reliable blocking range for half of the period (transmitting and blocking state.) To determine if the blocking duty factor is indeed 50 %, the difference between the position of rising and falling edges is calculated, resulting in table 2.1.

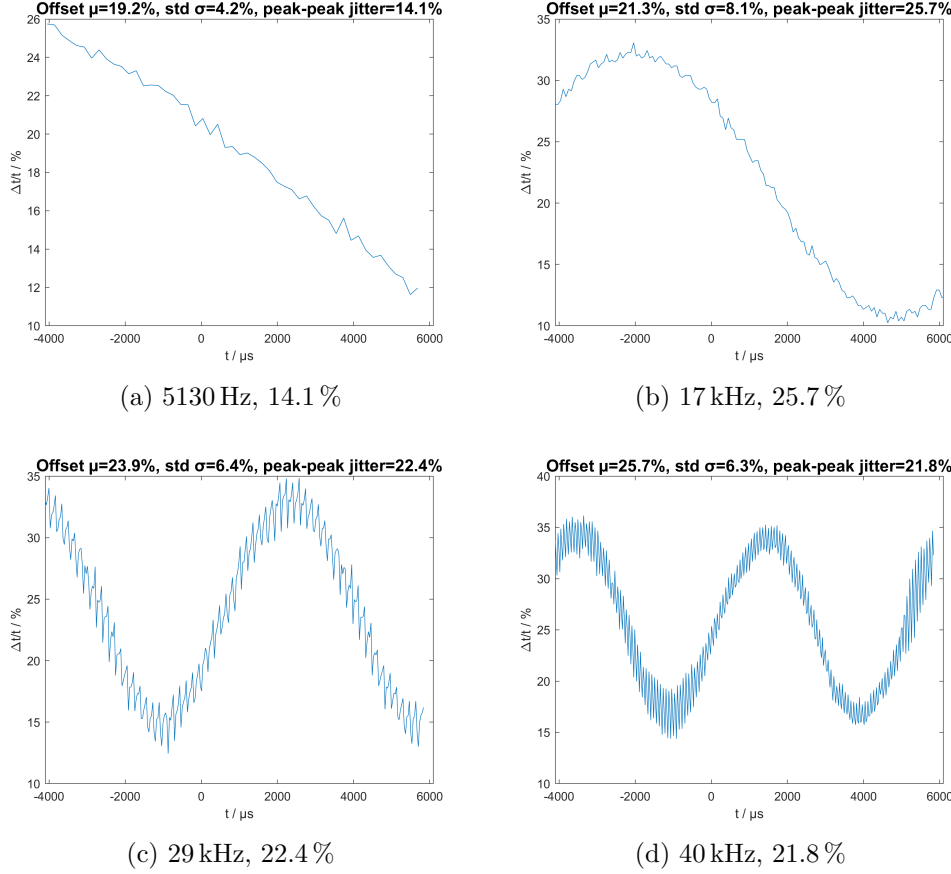


Figure 2.6.: Phase between reference signal and laser intensity on the photodiode when calibrating the chopper. Captions denote chopping frequencies and peak-to-peak jitter over a whole period. Table vibration may have contributed to the jitter.

To align pump pulse arrival time on the chopper and the synchroniser, Pharos laser's capability of delaying its SYNC2 output with respect to the laser pulse is used. The laser has an integrated pulse picker capable of only emitting every n -th pulse, effectively reducing the repetition rate. Note that the SYNC2 output does not change with the

Frequency / kHz	Full duration / μs	Positive duration / μs	Ratio / %
5.13	194.7(6)	107.2(9)	55.1(5)
17	71.1(3)	39.1(5)	55.0(9)
29	33.7(6)	18.4(8)	54.7(26)
40	24.9(6)	13.38(5)	53.7(29)

Table 2.1.: Positive half cycle duration and total chopping duration at different frequencies. Ratios are calculated per piece, uncertainties are standard deviations.

pulse picker setting, resulting in the full repetition rate being output instead of the whole fraction set and allowing the following algorithm:

1. Detect pump signal only on the detector
2. Repeat:
 - a) Set SYNC2 delay to a new value between 0 μs and 25 μs (full repetition period at 40 kHz)
 - b) Set pulse picker to 1, compare 20 kHz signal intensity to that at pulse picker of 2

Two cases can be worked with: Total extinction if Pharos pulse picker and chopper block pulses alternatingly or full transmission if they block the same pulse. For pump-probe measurements, what changes between these cases is the order of pulses, inverting the transient transmission ΔT_2 and turning the sign of the transient absorbance ΔA :

$$\Delta T_1 = \frac{I_{\text{probe}} + \Delta I_{\text{pump,probe}}}{I_{\text{probe}}} \Rightarrow \Delta T_2 = \frac{I_{\text{probe}}}{\Delta I_{\text{pump,probe}} + I_{\text{probe}}} \\ \Rightarrow \Delta A_2 = -\Delta A_1 = -1000 * \log_{10}(\Delta T_2)$$

2.3. History of the setup

2.3.1. Polarisation

SQIB samples investigated during this master thesis show a high dependency of transmissivity, transient absorbance and excited states on the input polarisation. This necessitates strict control over the linear polarizations used for both pump and probe beams, individually. Both NOPAs emit horizontally polarised light whose plane can be selected using achromatic $\frac{\lambda}{2}$ plates; likely, the spectrum of the laser pulses alone would make the use of zero-order or multiple-order waveplates unsuitable due to their strict wavelength requirements.

First measurements were performed using an achromatic 690 nm to 1200 nm $\frac{\lambda}{2}$ plate in combination with an ultra-broadband wire grid polariser (250 nm to 4000 nm). While this does provide control over power and polarization of both beams, the polariser also changes the transmitted intensity with each new setting. In particular, polarization scans and switches to new domains with different crystal orientations were too time-consuming and did not allow for minimum/maximum settings for each wavelength, but only relative directions by measuring the intensity transmitted by the $\frac{\lambda}{2}$ plate and the polariser in series. For this reason, a second $\frac{\lambda}{2}$ plate (400 nm to 800 nm) was bought and inserted in place of the wire grid polariser.

It should be noted that some measurements, particularly at 650 nm for pump and probe, are made outside the specified range of the 690 nm to 1200 nm $\frac{\lambda}{2}$ plate. However, the capability of blocking close to 100 % of power using a wire grid polariser shows that the beam is still linearly polarised.

2.3.2. Detection

For fast intensity detection, custom detectors are utilised. A Hamamatsu S1336-8BK photodiode is negatively biased at 4 V to 4.5 V and its output voltage is amplified using fast JFET operational amplifiers. To broaden the pulses in time in order to have more samples for pickup by the A/D converter, a low-pass filter is used. In first experiments, the whole circuit was soldered onto perfboard, put inside a cardboard box for optical shielding and detected using individual cables, but following versions were built on custom PCBs and put inside metal cases with BNC connections. As of this thesis, users can choose between a linear, symmetric power supply, NiMH accumulators and batteries for powering the detectors, enabling some portability as well as ease of use for more fixed positioning. Reference [10] contains a detailed description of the detector.

2.4. Spectra of the NOPAs

Due to the Heisenberg uncertainty principle $\Delta E \Delta t > \frac{\hbar}{2}$, for pulse durations sometimes as low as 30 fs, the spectrum of the laser needs to be relatively broad. Also, adjustments after initial setup of the NOPAs as well as drifts of the positioning inside the devices lead to offsets between the wavelength set and the central wavelength being emitted. Examples can be found in figure 2.7.

Figure 2.7 shows some NOPA spectra at central wavelengths of 650 nm and 740 nm, in part including the settings used to achieve the wavelengths desired.

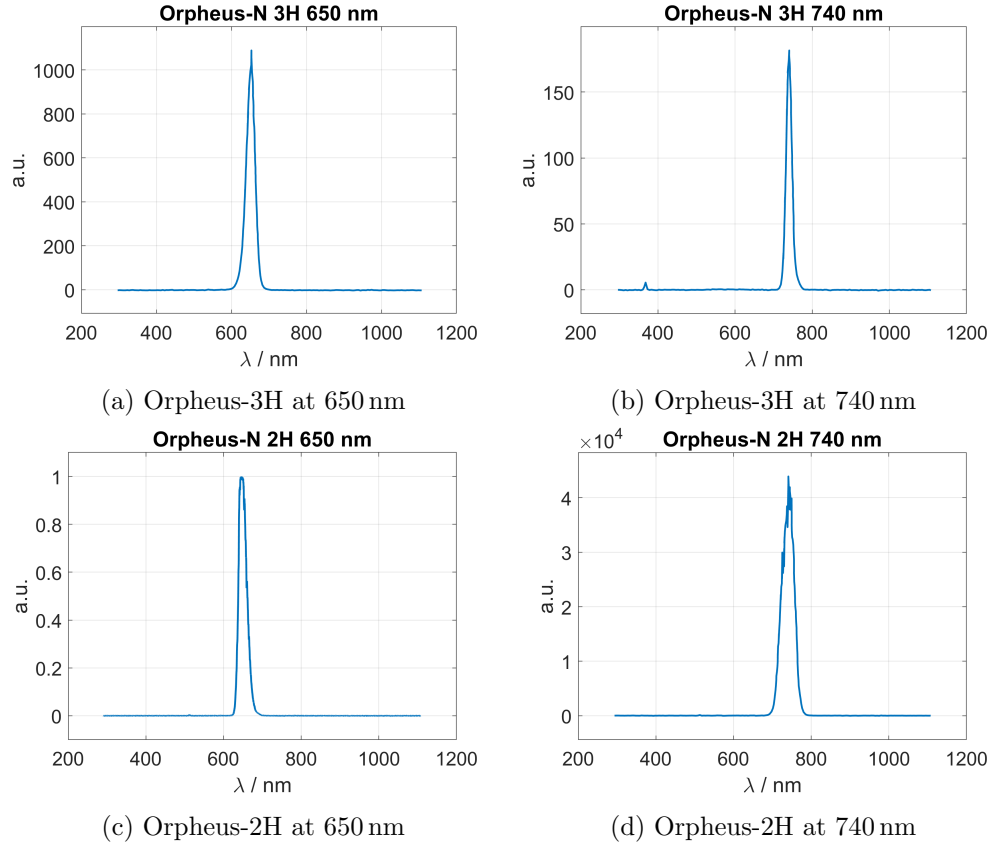


Figure 2.7.: Frequently used spectra for measurements. Central wavelengths in this Master thesis are set to be within 1 nm of the desired wavelength, often less than 0.3 nm as shown in the program are possible. Partly created with Web Plot Digitizer <https://apps.automeris.io/wpd/>. Remaining SHG/THG signal as present in b is filtered using glass long-pass filters if necessary.

2.5. Spatially separated pump-probe (SSPP)

Spatially separated pump-probe measurements (SSPP) can observe the transfer of excitations or charge carriers within the material by spatially shifting pump and probe beams with respect to each other. Preparations to enable SSPP measurements on the transient absorption microscope were undertaken for this thesis consisting of alignment measurements and proof-of-concepts using a CW laser.

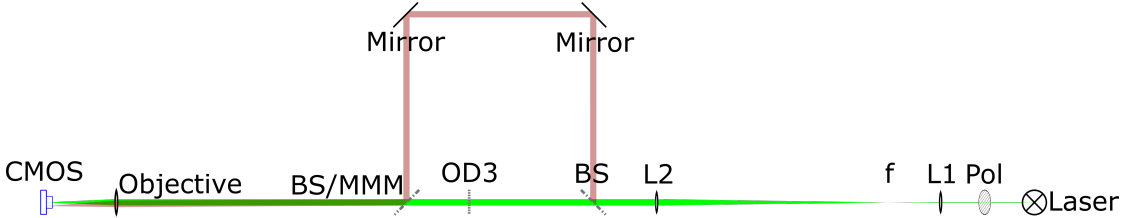


Figure 2.8.: Spatially separated pump probe calibration setup. Laser: Thorlabs PL203 laser diode, Pol: Thorlabs WG25M-UDB wire grid polariser, L1 and L2: $\approx 3 : 1$ telescope, BS: microscopy slide as beam splitter, OD3: neutral density filters, BS/MMM: motorised mirror mount with mounted microscopy slide, Objective: Olympus UPlanFL N 10x (NA = 0.3) objective

For measurements where charge and energy transfer can be expected further than the diffraction limit, calibration measurements for spatially separated pumping and probing are taken. The setup is explained in figure 2.8. The alignment works as follows:

1. The beam from the laser module is attenuated using a wire grid polariser.
2. It is then widened using a Galilean telescope comprised of two biconvex lenses placed apart $f_1 + f_2$. This is done to get closer to the diffraction limit of the objective by utilising its numerical aperture better.³
3. Part of the widened beam is reflected at the surface of a microscope slide used as a beam splitter. This part could be the probe beam in a real setup.
4. The other part is attenuated using an OD3 neutral density filter to approximately match the intensities.
5. A motorised mirror mount consisting of Thorlabs Z825B actuators mounted to a manual mirror mount combines both beams. Mirrors and motorised mount are set to achieve colinear beams.

By changing the position of the actuators, the angle of incidence of one of the beams onto the objective can now be varied with respect to the other beam. This results in linear movements on the focus plane of the objective and offsets on the camera. In a real transient setup, both beams would come from separate NOPAs and be focused into

³For smaller aberrations and a better beam quality, aspherical lenses or similar types could be used.

a colinear beam directly before the focussing objective. While there are no direct result from building this setup, it shows the feasibility of using the actuators for mirror tilting and spatially separated measurements.

Using a similar setup depicted in figure 2.9, albeit with only one beam and using an aluminium mirror instead of a microscope slide in the motorised mount, images are taken while moving the actuators over a range of values. Laser spot positions are determined on the image using the `D2GaussFitRot` (see reference [14]). These can then be fitted using a linear 2-dimensional model to the actuator positions:

$$\mu_x = A_{xx}x + A_{yx}y \quad (2.6)$$

$$\mu_y = A_{xy}x + A_{yy}y \quad (2.7)$$

where μ denote the peak position on the camera, x, y denote the position of the corresponding actuator and A is the transformation matrix. Ideally, A_{xy} and A_{yx} would be 0, indicating independent movement of the coordinates; in practice, however, they show about 1 % of influence on the other axis when compared to moving the other actuator (see table 2.2).

Table 2.2.: Calibration factors for the motorized mirror mount. How to read: 1 mm of offset on the horizontal actuator gives -6751 px of horizontal offset and 65 mm of vertical offset on the camera. Distances along the beam path can be seen in figure 2.9.

	$\Delta x / \text{px mm}^{-1}$	$\Delta y / \text{px mm}^{-1}$
x actuator	$-6751(5)$	$65(7)$
y actuator	$-55(12)$	$-6303(15)$

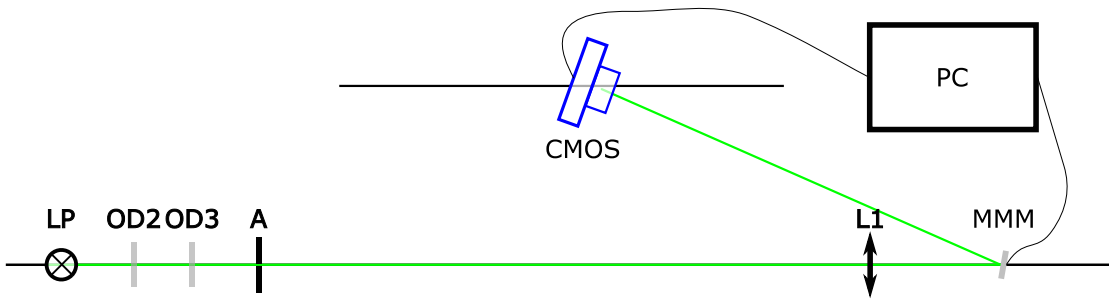


Figure 2.9.: Setup for calibrating the motorized mirror mount on two parallel optical benches (distance $d = 16$ cm). LP: Laser pointer ($\lambda \approx 520$ nm, 0 cm), OD2, OD3: Neutral density filters (6.5 cm, 11.5 cm), A: Aperture (18.5 cm), L1: LiF₂ lens ($f = 500$ mm, 72.5 cm), MMM: Motorized mirror mount (mirror holder, Thorlabs Z825B actuators with K-Cubes KDC101, PYREX aluminium-coated mirror, 84.5 cm minus 1.5 cm to mirror), CMOS: DMK 42AUC03 camera (pixel size 3.75 μ m, distance to mirror 39 cm). All distances ± 0.3 cm.

3. Methods

3.1. Transient absorption (TA)

In this thesis, the transient absorption technique is applied with shot-to-shot measurements achieved with an optical chopper (SciTech 310CD). The shot intensities are comprised of multiple components:

$$I_1 = I_{\text{probe}} + c_{\text{block}} * I_{\text{pump}} + \Delta I_{\text{pump,probe}} \quad (3.1)$$

$$I_2 = I_{\text{probe}} \quad (3.2)$$

where c_{block} is defined as the transmittance of stray light through mechanical blocks and optical filters. I_1 and I_2 describe the intensity of every odd and even shot, I_{probe} is the intensity of a single probe pulse, I_{pump} of a single pump pulse and I_{TA} the resulting change in probe intensity due to the interaction with the material. In this TA setup, I_{TA} is the only variable that become negative as will be described in other chapters.

The resulting data is recorded as

$$\Delta T = \frac{I_1}{I_2} = \frac{I_{\text{probe}} + c_{\text{block}} * I_{\text{pump}} + \Delta I_{\text{pump,probe}}}{I_{\text{probe}}} \quad (3.3)$$

As in the introduction section 3.5, a choice is made to calculate the transient absorbance:

$$\Delta A = -1000 * \log_{10}(\Delta T) = -1000 * \log_{10} \left(\frac{I_1}{I_2} \right) \quad (3.4)$$

resulting in positive values meaning that the material becomes more opaque due to the pump pulse whereas negative values mean that the material becomes more transparent. As a sanity check for the correct sign in measurements, the sign of ΔA (given in mOD) should always be negative on the probe-pump side as, after 25 μs from the last pulses (25 $\mu\text{s} \gg 250$ ps of maximum delay), their effect can be neglected:

$$I_{\text{TA}} \approx 0 \Rightarrow \Delta T = 1 + \frac{c_{\text{block}} * I_{\text{pump}}}{I_{\text{probe}}}$$

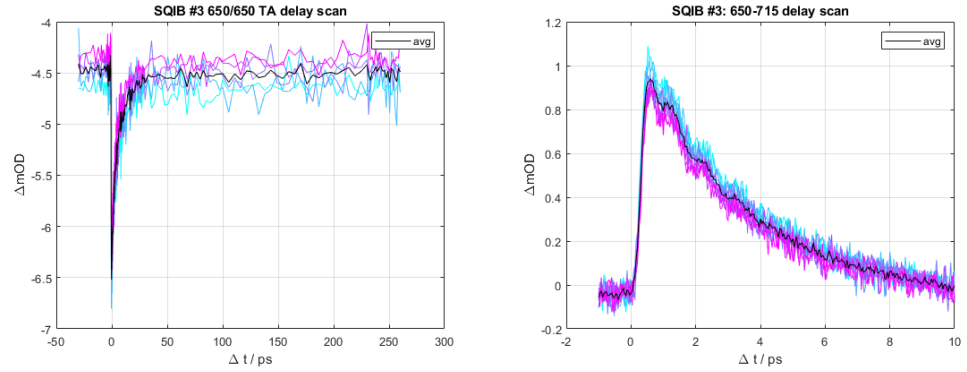
and there should only be additional intensity due to unfiltered pump light hitting the detector in addition to pump light.

Filters such as 700 nm interference longpass and shortpass, as well as some glass filters for other wavelengths make it possible to remove pump components almost completely while mechanical beam blocks and the movement of the pump focus off the detector can be used to partially block pump light. See figure 3.1 for a comparison. Mechanical

blocking can be performed straight after the second objective and by moving the pump pulse away from the detection surface using the focussing mirror, achieving up to two orders of magnitude of pump pulse extinction.

However, since pump-probe and probe-only pulses can not be distinguished in algorithms or by looking at the input signal, putting the stage in a probe-pump position and looking for the transient signal provides a reliable way to determine if the order is set correctly: since remaining pump light increases the intensity measured at the photo detector, a correct trigger should *decrease* the transient absorbance:

$$c_{\text{block}} * I_{\text{pump}} > 0 \Rightarrow \Delta A < 0$$



(a) 650 nm pump, 650 nm probe, UDB/UDB measurement on SQIB 3: mechanical blocks only
(b) 650 nm pump, 715 nm probe, UDB/LDB measurement on SQIB 3: FELH0700 interference filter

Figure 3.1.: Comparison between interference filtering and mechanical filtering. A difference in TA intensity especially on the probe-pump side to the left of the overlap peak is visible. (4.5 mOD vs. 0 mOD of background)

3.2. Scan modes

Due to many degrees of freedom, the transient absorption microscope allows different scan modes. In the following list, those modes used in this master thesis and one that may be utilised in the future can be seen:

- Single TA delay scan: Pump and probe are active, delay stage is scanned and transient absorption is collected for each delay step. To check for variations in power and sample degradation, 20 kHz and 40 kHz signals are also recorded individually.
- TA delay scan series: In order to create some statistics for each point, single TA time scans are repeated multiple times.
- TA sidestepping scan: A specific measurement is repeated at multiple spots in the same domain. This helps in detecting sample degradation particularly when high

intensities are applied. However, TA intensities often show differences within the same platelet.

- **Imaging scan:** The delay stage is set to a specific position (e.g. first maximum in transient absorption) and the sample is scanned in X and Y directions. This both creates an image of transmitted single-pulse intensity and the transient absorption at every spot, resulting in an image.
- **Cross-sectional scan:** TA time scans are performed along some line on the sample. The target is to identify correlations between TA intensity, decay constant and other parameters and the sample position. This technique could also be used on a 2-dimensional surface.
- **TA polarisation scan:** For a set of pump or probe polarisations (the other one is most often set to maximum or minimum transmission), a single TA time scan is performed.
- **TA transmissivity scan:** With only one of the lasers enabled, the dependency of transmitted intensity over incident polarisation is recorded one or multiple times (for statistics).
- **Spatially separated pump-probe scans (SSPP):** Instead of moving the sample, only one of the lasers is moved from its center position. This technique was originally planned for this thesis and may be implemented in further experiments. See reference [7] and related papers for a more in-depth description and applications.

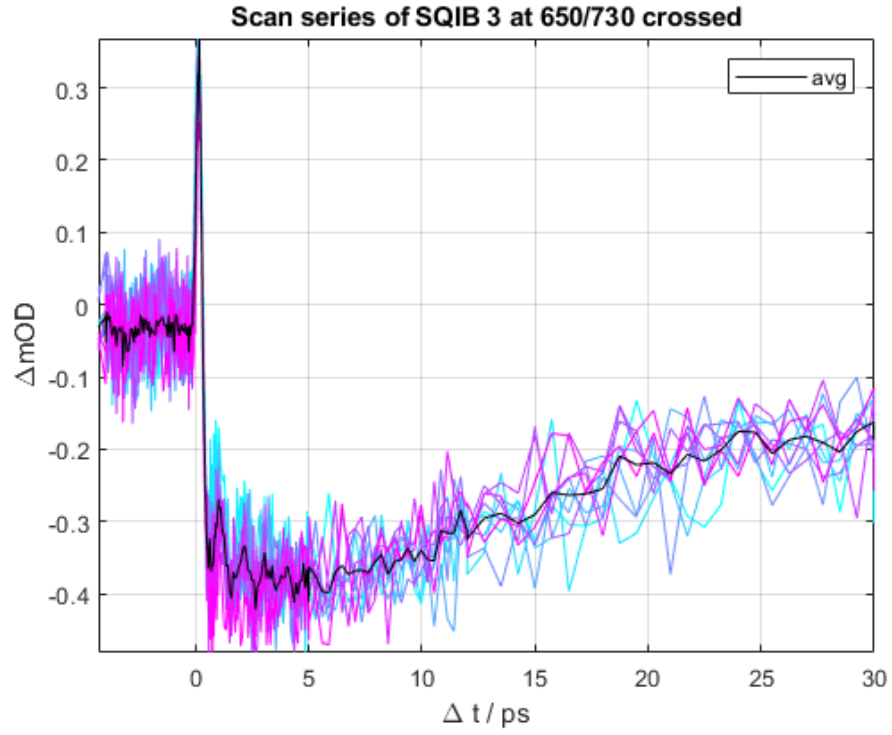
3.3. Microscopy and scaling

Before taking TA measurements, it is important to find a suitable spot within a platelet on the sample and to align pump and probe beams to achieve optimum spatial overlap. This is achieved by placing an LED light source before the first objective, aligning the second objective to the surface under investigation and checking if the image changes when moving the sample actuators.

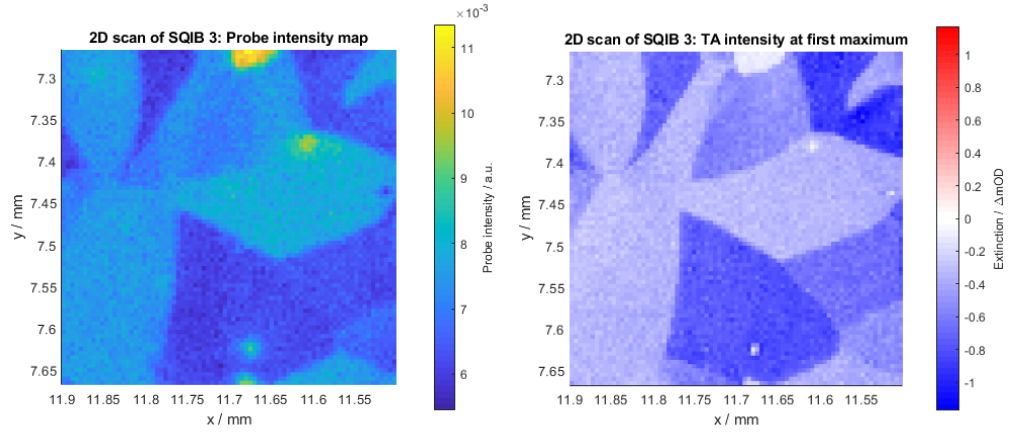
Since the actuators are connected to the sample holder with a 1:1 transmission, their set position directly corresponds to the position of the sample. This can be used to determine the scaling of the microscope: Overlapping images are taken from a region on the sample. They are then aligned using GIMP (of course, other image manipulation software with layer capabilities may be used) and the difference in pixels is recorded. The calculated factor between a pixel on the camera and the actuator position is:

$$1 \text{ px} = 233(10) \text{ nm} \quad (3.5)$$

It should be noted that, in the setup described in this Master thesis, the camera is particularly prone to being illuminated at a horizontal angle $\neq 90^\circ$ due to the rotation



(a) TA scan series: Cyan to magenta curves are individual measurements (ordered by measurement time) and show high amounts of noise whereas the black average line shows much more detail especially around the oscillations.



(b) 2D scan: Transmitted intensity

(c) 2D scan: Transient absorption at first maximum

Figure 3.2.: Scan modes of the transient absorption microscope

of its case. For this reason, the factor in section 3.3 is calculated from the vertical axis where the mounting mechanism ensures straight illumination and the horizontal scale bar on microscopy images may be longer than shown in some cases. However, this is not true for the scanned images in TA microscopy as the sample is moved physically.

3.4. Spatial overlap and point spread function

After determining a suitable spot for transient absorption measurement, the next step is to align pump and probe beams on the sample. While the second objective is still set to produce a sharp image of the sample surface on the camera, the LED light is removed from the beam path and both pump and probe beams are directed towards the sample. Laser alignment paper is used to ensure good parallelism of both beams upon entering the first objective. Both spots should then be visible on the camera. By varying the position of the first objective along the laser beam axes, the spot size can be set on the sample.

While achieving maximum resolution by putting the sample surface directly in the focus of the first objective may seem desirable, this is often not the case for SQIB sample as they are prone to deterioration highly dependent on the peak radiance. For this reason, a program `liveFit.m` is written to fit a Gaussian function to a beam spot recorded with the camera according to the following algorithm:

1. Insert neutral density filters and use IC Capture software to set settings that utilise the bit depth of the camera without saturating.
2. Access the camera via the Matlab webcam plugin
3. Repeat every second:
 - a) Acquire an image from the webcam
 - b) Remove all pixels at their maximum intensity to remove dead pixels on the camera sensor (optionally; can be switched off for laser spots saturating the sensor, albeit with less exact FWHM results)
 - c) Do a Gaussian fit across the sum of all rows and columns to determine good starting parameters for a cross-sectional fit
 - d) Select cross-sections at the center positions of both Gaussians, do another Gaussian fit
 - e) Draw the image with scaled colors and show the selected cross-sections
 - f) Display position of the cross-sections and the peak width as well as the calculated FWHM (full width, half maximum) and the peak radiance calculated from the total input power and the Gaussian model

The model used is a simple Gaussian PDF:

$$I(x) = \frac{I_0}{\sqrt{2\pi}\sigma_x} \exp\left(-\frac{(x-x_0)^2}{\sigma_x^2}\right) \quad (3.6)$$

$$I(x, y) = \frac{I_0}{2\pi\sigma_x\sigma_y} \exp\left(-\frac{(x-x_0)^2}{\sigma_x^2} - \frac{(y-y_0)^2}{\sigma_y^2}\right) \quad (3.7)$$

$$FWHM = 2\sqrt{2\log 2}\sigma \quad (3.8)$$

$$I_{\text{peak}} = \frac{P_{\text{total}}}{2\pi\sigma_x\sigma_y} \quad (3.9)$$

where the peak intensity I_{peak} is derived from the area of the 2-dimensional Gaussian function: $P_{\text{total}} = \int_{-\infty}^{\infty} \int_{-\infty}^{\infty} I(x, y) dx dy$, $I(x=0, y=0) = \frac{I_0}{2\pi\sigma_x\sigma_y}$. 1-dimensional functions are used for fitting whereas the 2-dimensional model is relied upon for all other calculations (peak intensity I_{peak} and full width half maximum $FWHM$.) An example for the `liveFit` interface can be seen in figure 3.3. Note that the total power P_{total} has to be measured beforehand using a laser power meter as the camera resolution of 8 bit would be too low and the influence of ambient light too high for a direct measurement.

Whereas the calculated beam position is particularly useful for observing beam movement during stage usage or NOPA wavelength changes, the $FWHM$ is related to the spatial resolution on the sample surface and the peak intensity is a measure for how fast the spot is destroyed by laser exposure.

3.5. Fit model for state population

For a clear description of femtosecond dynamics, a mathematical description of multiple decays is needed. Reference [9] contains a detailed derivation for calculating the population of excited state after laser excitation based on the convolution of a Gaussian laser pulse with exponentially decaying excitations, including population transfer between different states.

According to the reference, a normalised model function for a single exponential decay is:

$$N(t; \tau, \sigma) = \frac{1}{2} \exp\left(-\frac{\sigma^2}{2\tau^2}\right) \left(2 - \text{erfc}\left(\frac{t - \frac{\sigma^2}{\tau}}{\sqrt{2}\sigma}\right)\right) \exp\left(-\frac{t}{\tau}\right) \quad (3.10)$$

with N population, t time after excitation, \exp exponential function, erfc complementary error function, σ laser pulse duration, τ decay constant.

A total signal could, for example, be fitted according to the following equation:

$$N_{\text{sum}}(t) = \sum_{i=1}^n A_i N(t - t_0; \tau_i, \sigma) + k(t - t_0) + d \quad (3.11)$$

A_i is the amplitude of the i^{th} excitation, N the function outlined in equation (3.10) and k and d constants of a linear background. The linear subtraction can be necessary if there is a parallel offset due to the delay stage movement; in other cases, a constant offset

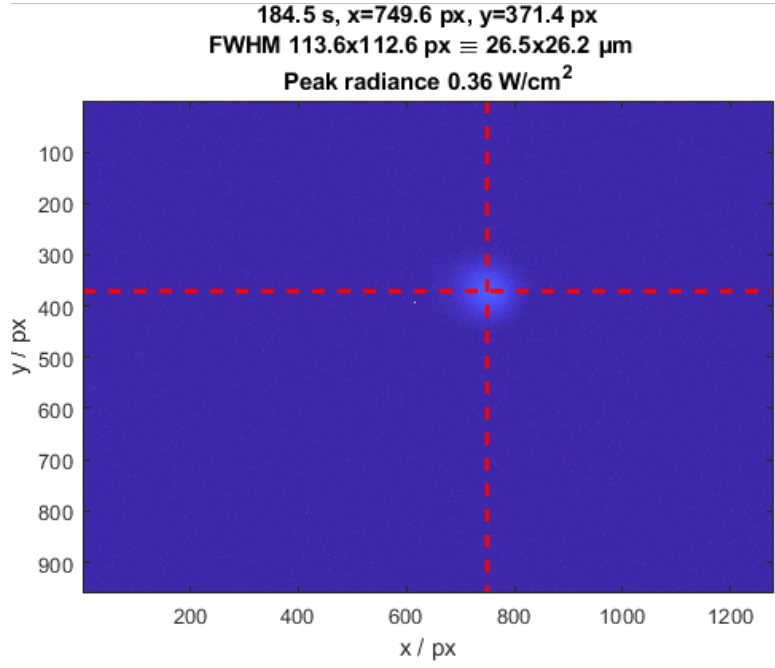


Figure 3.3.: liveFit/beam profiler interface. Top line: Time elapsed, central position of the beam, middle line: Full width, half maximum in pixels and μm , bottom line: peak radiance according to a 2D Gaussian distribution. In this case, the program was used to remove parallel offset in beam position when moving the stage.

d can suffice. Generally, the positions of the mirrors on the delay stage are optimised to avoid beam movement.

4. Samples

4.1. Molecular crystals

This section is based on reference [16, chapter 1], citing the most relevant parts for this Master thesis. For the purposes of this thesis, a molecular crystal is defined as an organic solid that is arranged as a single crystal or as polycrystals. Molecular crystals typically exhibit excitonic states with energies below that necessary for the excitation from the valence band into the conduction band. They are termed Frenkel excitons and show as bound electron-hole pairs capable of transporting energy; compared to molecular states in the gas phase, one needs to include interactions with neighbours and other molecules within the crystal lattice. A theoretical description is given in reference [11, chapter 1].

In particular, the samples under investigation are part of the group of charge-transfer crystals as shown in the molecular structure in reference [2], having a Donor-Acceptor-Donor configuration (DAD).

4.1.1. Davydov splitting

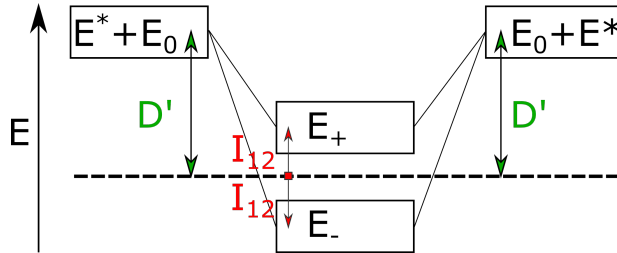


Figure 4.1.: Energy scheme of Davydov splitting in case of dimers. $E_0 + E^*$ is the energy of an excited molecule and a molecule in its ground state, D' the constant shift due to attractive interaction and I_{12} the Davydov splitting from D' .

This subsection is a summary of the corresponding section in reference [4]. As figure 4.1 shows, Davydov splitting can be introduced by assuming two interacting, identical molecules 1 and 2, forming a dimer and having wavefunctions ϕ_1 , ϕ_2 and energies $E_1 = E_2 = E_0$. The total ground state is then given by $\Phi_G = \phi_1\phi_2$ and $E_G = 2E_0$. When one of the molecules is excited (ϕ_i^*), the wavefunction changes to

$$\Phi_{\pm} = \frac{1}{\sqrt{2}}(\phi_1\phi_2^* \pm \phi_1^*\phi_2) \quad (4.1)$$

Interaction introduces two additional terms to the dimer energy:

$$E_{\pm}^* = E^* + E_0 + D' \pm I_{12} \quad (4.2)$$

where E^* is the energy of one excited molecule, D' is a static shift called *Coulomb interaction energy* and $2I_{12} \equiv \Delta_D$ is called the *Davydov splitting*.

The polarisation of the optical transitions in the two Davydov components is determined by the transition dipole moments \vec{M} in the case of allowed optical transitions. In case of a dimer, a total transition moment is

$$\begin{aligned} \vec{M}_{S_1 \leftarrow S_0} &= \langle \Phi_G | e\vec{r} | \Phi_{\pm}^* \rangle \\ &= \frac{1}{\sqrt{2}} \langle \phi_1 \phi_2 | e\vec{r} | \phi_1 \phi_2^* \pm \phi_1^* \phi_2 \rangle \\ &= \frac{1}{\sqrt{2}} [\vec{M}^2 \pm \vec{M}^1] \end{aligned} \quad (4.3)$$

meaning that, in case of parallel molecules, only one of the transitions is optically allowed as the other transition moment is $\vec{M}_{-}^{dimer} = \vec{0}$. Other cases allow two optical transitions with distinct energy and polarisation. The maximum number of Davydov states is the number of molecules in the unit cell.

4.2. Squaraines and SQIB

2,4-Bis[4-(N,N-diisobutylamino)-2,6-dihydroxyphenyl]squaraine, in short SQIB from Squaraine and Isobutyl side chains, is an organic compound. Figure 4.2 shows the structure of the molecule under investigation. In molecular crystals, the side chains are sometimes responsible for the molecular arrangement according to reference [11]; in this case, the Isobutyl chain allows the formation of monoclinic and orthorhombic modifications depending on the preparation conditions.

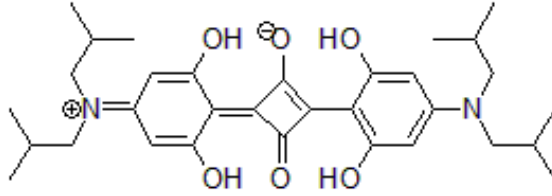


Figure 4.2.: 2,4-Bis[4-(N,N-diisobutylamino)-2,6-dihydroxyphenyl]squaraine (SQIB) molecular structure, provided by Manuela Schiek. \oplus and \ominus show ions within the molecule; the positive charge can also exist at the other nitrogen atom or in a partially charged cyanine form as explained in reference [2].

Most measurements, apart from those used for the introduction of new elements to the transient absorption microscope, focus on the exciton dynamics and on imaging SQIB

samples. The SQIB samples under investigation are oriented in an orthorhombic crystal lattice with the following lattice constants as per reference [2]:

$$\begin{aligned}a &= 15.0453(8) \text{ \AA} \\b &= 18.2202(10) \text{ \AA} \\c &= 10.7775(6) \text{ \AA} \\Z &= 4\end{aligned}$$

The (110) plane is oriented parallel to the surface in the samples under investigation which is relevant for the orientation of transition dipole moments as described later in this section.

As described in reference [2], orthorhombic platelets can be grown by dissolving the substance in amylene stabilised chloroform (trichloromethane), spin-coating onto cover-slip glass at 1500 min^{-1} for 60 s and annealing on a hotplate for 180°C for 2 h, all in a nitrogen-filled glovebox.

The resulting samples consist of platelets with diameters of approximately $10 \text{ }\mu\text{m}$ to $200 \text{ }\mu\text{m}$. They show strong Davydov splitting with peaks at 640 nm and 730 nm and intersecting bands of upper and lower Davydov bands as can be seen in their spectra in figure 4.3.

Due to the non-parallel alignment of molecules within the unit cell (see reference [13]), there are also at least two distinct transition moments for upper and lower Davydov bands. The lower band is along the crystallographic c -axis (molecular stacking direction) and the upper Davydov component is along the projection of the b -axis onto the (110) plane according to reference [2]. The (110) plane is parallel to the substrate surface, thereby explaining the *perpendicular orientations* of the projected transition dipole moments as observed in reference [2] and the experiments done throughout this Master thesis. This selectivity depending on the light polarisation leads to the definition of a nomenclature to describe the excited state:

- p_{LDB} (lower Davydov band/component) polarisation: Linearly polarised light where the majority of excitations is expected to happen with lower band.
- p_{UDB} (upper Davydov band/component) where most of the excitations are expected within the upper band

Unless explicitly stated, this nomenclature is used throughout this thesis when explaining the excitation of select states within the SQIB sample.

While preparation itself was done by the Schiek group under the conditions described, the actual experiments were performed under ambient conditions. Figure 4.4 shows microscope images of SQIB sample 3 between crossed polarisers. It is clearly visible that there are distinct platelets, some of them have very uniform orientations such as in figure 4.4a, others show a greater variation as can be seen in figure 4.4b which also contains less uniform or damaged spots. For measurements, the LED light source is replaced with either of the NOPAs and spot position and a central spot on one of the platelets are aligned using the x-y stage. Using the camera preview, it is also possible to determine a range of similar spots in the same domain, allowing for measurement

series without photodamage between single measurements. Without crossed polarisers, the monochrome camera image only shows a uniform surface with small quantities of dust particles.

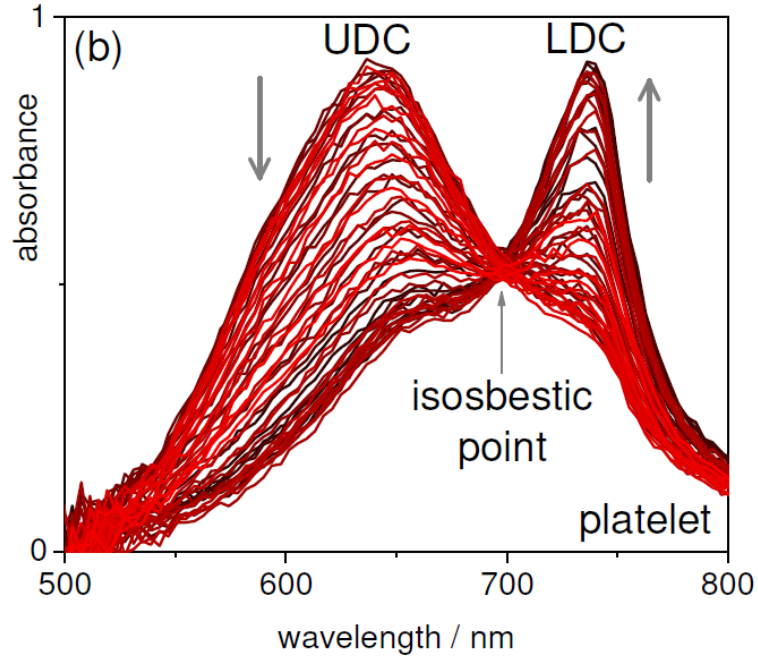
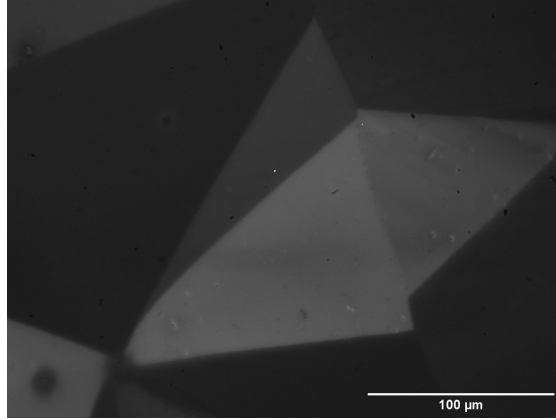
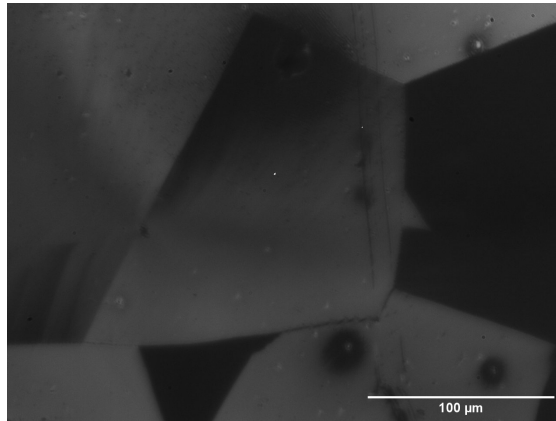


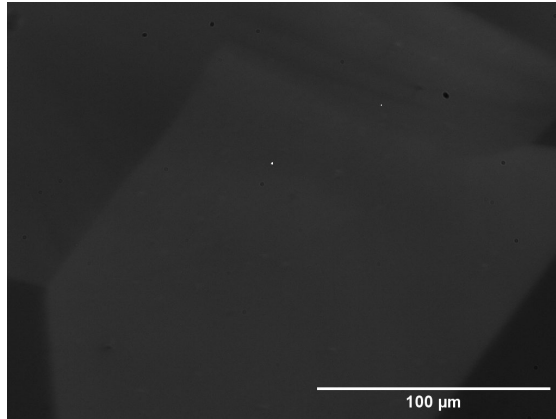
Figure 4.3.: Absorbance of an orthorhombic SQIB platelet recorded with a single polariser. The polarisation with the maximum peak at 740 nm is called LDB or LDC whereas the bright red curve with a maximum at 650 nm is called UDB or UDC throughout this thesis due their selectivity of the corresponding transitions. Source: Supporting material of reference [2].



(a) Small domains with widely different polarisations



(b) Defects (black spots). They sometimes happen if spot is exposed for too long, but exist on the untouched sample as well.



(c) Large domains. Good for having a set of points with very similar orientation to those affected by degradation.

Figure 4.4.: Various images of spots on the sample SQIB 3 between crossed polarisers. Contrast shows spatial differences in the polarizing properties of the sample in different domains.

4.2.1. Sample degradation due to photodamage

Due to some experience with quantum dot samples, first measurements on SQIB were performed at powers between $2\text{ }\mu\text{W}$ to $10\text{ }\mu\text{W}$ per laser corresponding to 50 nJ to 500 nJ per pulse. While this offers a great signal-to-noise ratio even without an optical chopper, degradation of the sample within a few minutes quickly becomes evident. Not only does the TA delay scans change shape (often showing the opposite behaviour in transient intensity change compared to a fresh spot), but optical microscopy of the sample shows bleached spots as well (figure 4.5). This figure shows three different phenomena associated with photodamage: Lighter or darker spots on polarisation microscopy images, a change in transient absorption delay scan shape over time and a complete change of transient signal behaviour, also in a set of delay scans.

Obviously, the first step to improving the reproducibility of measurements of one spot is to reduce the power of the laser. A choice is made to use $0.12\text{ }\mu\text{W}$ to $0.5\text{ }\mu\text{W}$ or 3 pJ to 25 pJ per pulse of usable power range; the upper end of this range was chosen for measurements with a low efficiency, e.g. LDB pumping below 700 nm . Measurements were taken to show the influence of both pump and probe intensity changes on the TA intensity curve. While the transient absorbance increases *linearly* with *pump* power, changes in *probe* power only show an influence on the *signal-to-noise ratio* of detector and oscilloscope. However, the ratio of pump and probe is relevant for the relative amount of scattered pump light hitting the detector which shows especially on the probe-pump side of TA delay scans.

The detection of deteriorating spots is possible in multiple ways. One of the most useful ways is to perform a measurement series on the same spot and look for changes in the decay curves; changes in peak intensity and background intensity are common, but we even observed transitions from excited state absorption to ground state depletion after long exposures. Another method that could be done is to separately record the probe beam intensity at every spot: A strong decrease in absorption is indicative of progressing deterioration.

Since there were two orthorhombic SQIB samples prepared in the same way, an attempt was made to reduce the amount of photodamage by gluing a cover slip onto the sample surface in an inert argon atmosphere (SQIB sample 6). In contrast, SQIB 3 remained uncovered and exposed to the normal atmosphere. As shown in the imaging section 5.3, this proved to be unsuccessful. This may be due to chemical reactions restricted to SQIB itself or because evaporation of the material was part of the deterioration; however, a change in decay time and contributing effects to the transient absorption curve shows that chemical reactions take place. Pure evaporation is expected to only change the transient absorbance contrast due to a lowering of the interaction volume.

Steps to detect and avoid degradation are:

- Minimizing pump and probe intensity to lower energy input
- Record probe intensity in addition to TA intensity for transmissivity comparisons over time
- Sidestepping: Varying the exact position for measurements within a single domain

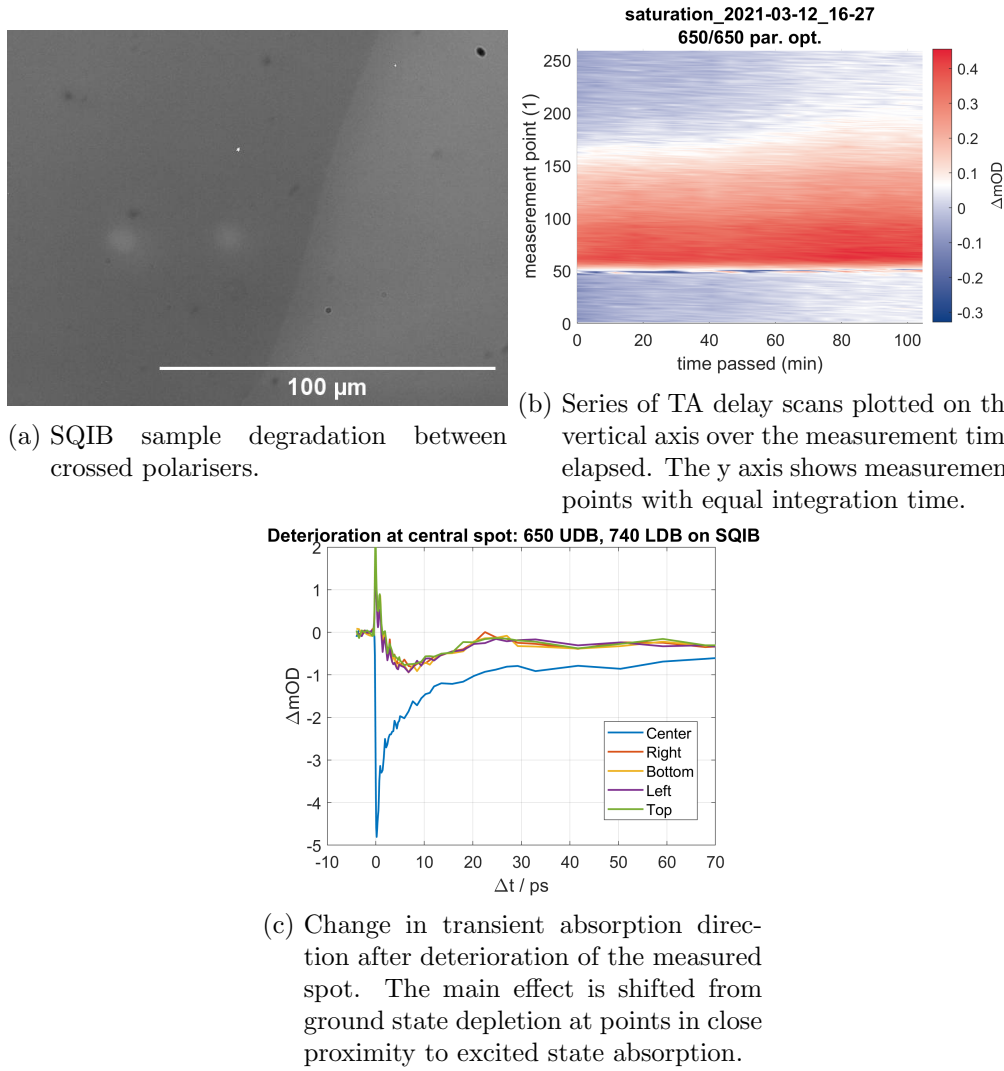


Figure 4.5.: Spot degradation on SQIB sample 6. As the domains act similarly to a polarisation filter, microscope images recorded with the sample being between crossed polarisers show either lighter or darker spots depending on the orientation of the polarisers as in a. b shows a significant elongation in decay time with the time elapsed during the laser exposure. c includes a delay scan of a central, photodamaged spot in comparison to delay scans directly adjacent within the same domain, including a complete change in transient absorption effects.

- Splitting of single measurements into measurement series to compare graph shapes

While very useful in principle, the sidestepping technique sometimes produces different results in close proximity, especially changes in the maximum transient absorbance ΔA and the absorption itself.

5. Results

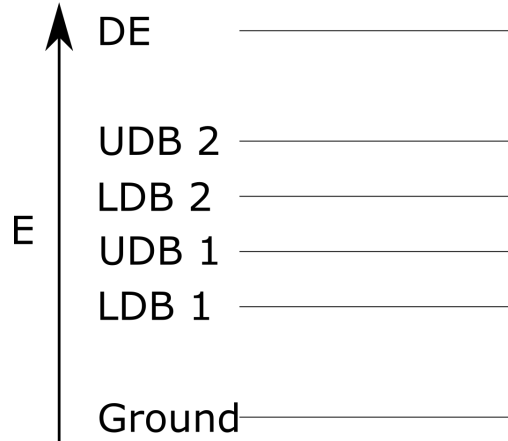


Figure 5.1.: Energy scheme of single and double excitations in SQIB. UDB 1 and LDB 1 are associated with single excited states in the dimer picture in 4.1.1, UDB 2 and LDB 2 with one of the molecules having a double excitation and DE with both molecules having a single excitation.

To accurately define measurements, there needs to be a common understanding of different sets of settings. We therefore define:

- Polarisation
 - p_{UDB} : Linear polarisation parallel to the Upper Davydov Band, assumed to be at minimum transmission through the sample at 650 nm according to calculations
 - p_{LDB} : Linear polarisation parallel to the Lower Davydov Band, assumed to be at minimum transmission through the sample at 740 nm
- Peak radiance
 - I_{peak} : Maximum of a 2D Gaussian function with a defined total power and amplitude, mean and standard deviation being fitted from a camera image of the laser spot
- Wavelength
 - Central wavelength as given by the spectrometer integrated into both of the NOPAs

- Wavelength setting in the software WinTOPAS differs from the central wavelength measured, so it is adjusted to achieve less than 1 nm of offset.

Where not stated otherwise, both pump and probe power are set to $0.25 \mu\text{W}$ with a peak radiance of $\approx 0.2 \text{ W cm}^{-2}$, equating to a pump energy of 15 pJ per pulse and a probe energy of 7.5 pJ per pulse. Probe may be varied between $0.2 \mu\text{W}$ to $0.3 \mu\text{W}$ for wavelength scans because, according to test measurements, this only influences signal-to-noise ratio, not the actual signal. Pump variations, on the other hand, do change the TA intensity and need to be set accurately for every measurement. Figure 5.1 shows a preliminary energy scheme as determined from measurements in upcoming sections.

5.1. Excited states: Zero-crossing points into excited state absorption

An important aspect of ultrafast microscopy is to find excited states that, with continuous illumination, cannot be reached due to the need for multi-photon processes (at which intensities SQIB samples would likely deteriorate within split seconds using CW light sources). This can be achieved by scanning the probe wavelength towards higher energies until excited state absorption is the dominant effect, indicating a state that can be reached via the combination of pump and probe excitation and an increase in the transient absorbance.

p_{UDB} probe As shown in figures 5.2 and 5.3, for p_{LDB} pumping, at wavelengths above 570 nm, ground state depletion dominates over other effects whereas at higher energies, there are states that can be excited efficiently via the combination with the first lower Davydov state and the upper probe polarisation. The corresponding measurement at 740 nm lower band pump, upper band probe wavelength scan in figure 5.3 looks similar, but with much less transient absorbance. From these sets of measurements, we conclude:

$$\lambda_{zc}(650 \text{ nm } p_{\text{UDB}} \text{ pump, } p_{\text{UDB}} \text{ probe}) = 530 \text{ nm} \quad (5.1)$$

$$\lambda_{zc}(740 \text{ nm } p_{\text{LDB}} \text{ pump, } p_{\text{UDB}} \text{ probe}) = 560 \text{ nm} \quad (5.2)$$

where λ_{zc} is the zero-crossing wavelength. It should be noted that there may be other zero-crossing points for each of these measurements beyond the capabilities of the NO-PAs in use. At 650 nm p_{UDB} pump, the change in transient absorbance is much more pronounced than at 740 nm p_{LDB} . Using equation (3.11) with one exponential decay, the decay constant is 4.9(1) ps at 740 nm p_{LDB} pump and 520 nm and 500 nm p_{UDB} probe; other curves of both sets of measurements do not have sufficient signal for fitting.

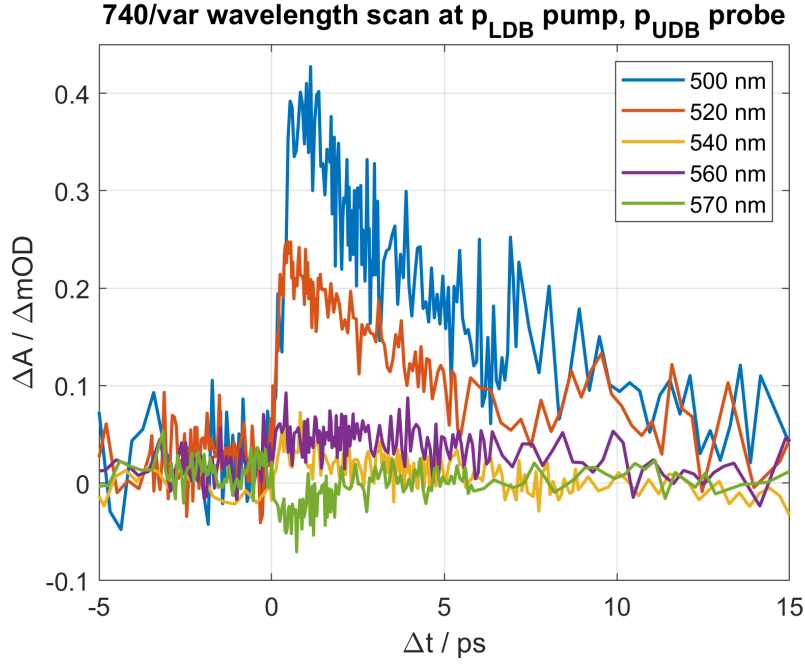


Figure 5.2.: Zero-crossing point from ground state depletion/stimulated emission to excited state absorption for 650 nm p_{UBD} pump and varied upper band probe wavelength. The signal at 560 nm almost vanishes, wavelengths below mainly result in excited state absorption, higher wavelengths only result in ground state depletion/stimulated emission. Measurements saturation_2021-06-23_18-53, saturation_2021-06-23_19-08, saturation_2021-06-23_20-45, saturation_2021-06-24_12-14

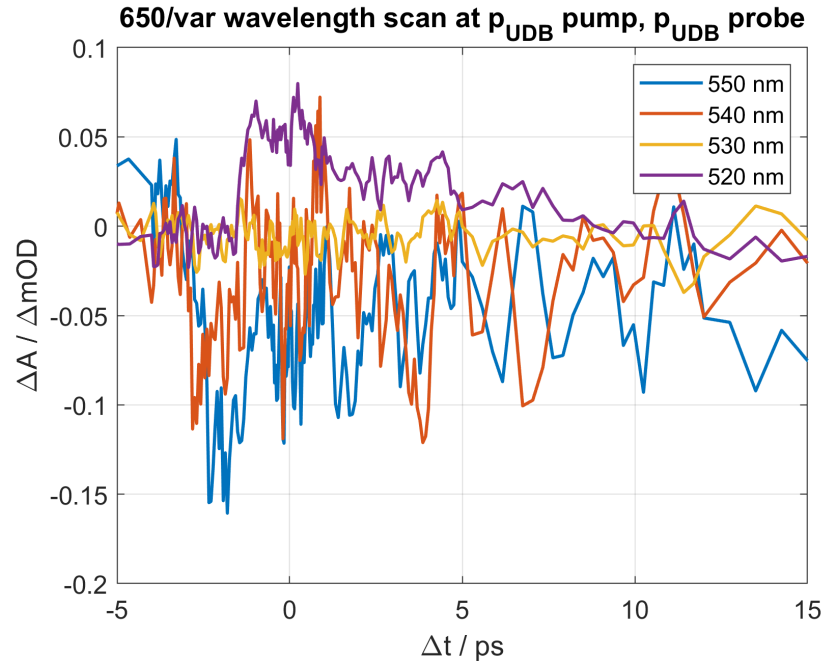


Figure 5.3.: Zero-crossing point from ground state depletion/stimulated emission to excited state absorption for 650nm p_{UGB} pump and varied p_{UGB} probe wavelength. Static background, appearing as offset on the probe-pump side, was subtracted. Note the direction of edges after the temporal overlap; at 530 nm, no step is visible, lower wavelengths result in excited state absorption and higher states only in ground state depletion/stimulated emission. Measurements 3933, 3932, 3931, saturation_2021-06-29_15-26, saturation_2021-06-29_17-03

p_{LDB} probe As shown in the image matrix figure 5.4, in contrast to the upper Davydov probe, zero-crossing points appear roughly at the same position for both 650 nm UDB pump and 740 nm LDB pump, transitioning from ground state depletion to excited state absorption at lower wavelengths:

$$\lambda_{zc}(650 \text{ nm } p_{\text{UDB}} \text{ pump, } p_{\text{LDB}} \text{ probe}) = 730 \text{ nm} \quad (5.3)$$

$$\lambda_{zc}(740 \text{ nm } p_{\text{LDB}} \text{ pump, } p_{\text{LDB}} \text{ probe}) = 730 \text{ nm} \quad (5.4)$$

meaning that there is a dominant second excited state at 3.35 eV, the energy of pump and probe photons combined, for p_{LDB} probing which is indicated as LDB2 in figure 5.5 and another excited state at 3.58 eV indicated as UDB2 in the same figure. It should however be noted that there are indications of a very fast relaxation of the UDB1 population into LDB1 as outlined in 5.8, meaning that the second excited state visible here would only be at 3.35 eV. When probing the lower Davydov state, oscillations as shown in section 5.1.1 are common, particularly in the range of 650 nm to 740 nm pump regardless of the polarisation.

Figure 5.5 shows an overview of the excited states that were gathered from the measurements. From the ground state, pumping can excite populations from the ground state into LDB1 and UDB1, followed by higher excitations into LDB2 and UDB2 as gathered from the p_{LDB} zero-crossing experiments. There is also a possibility for reaching a further excited state visible in the p_{UDB} probe zero-crossing measurements. No other zero-crossing points were observed in the available wavelength range of the NOPAs.

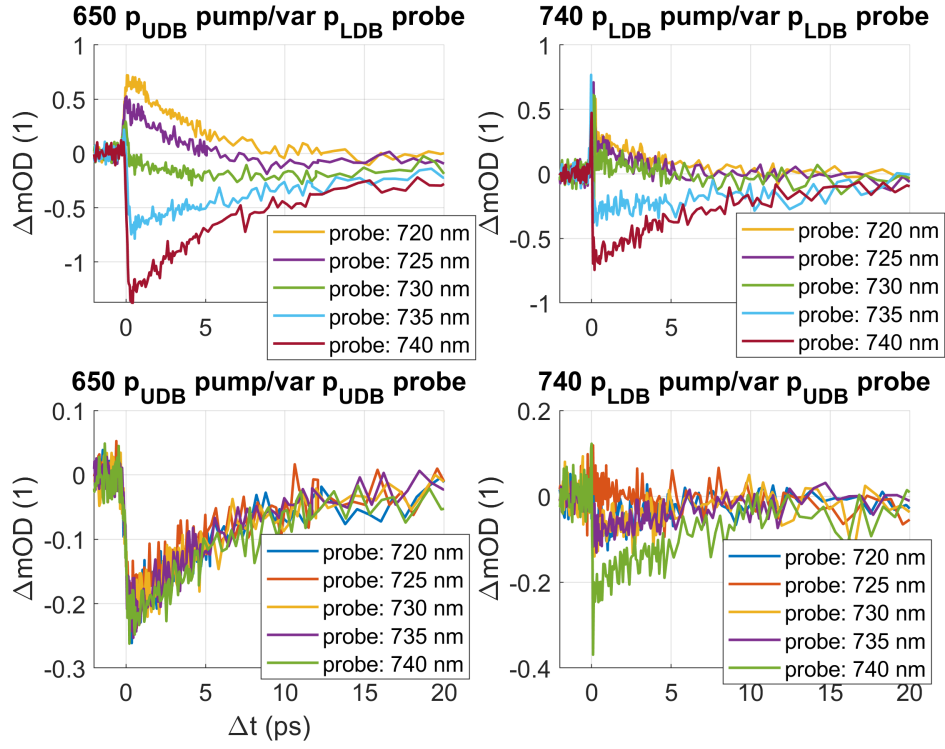


Figure 5.4.: Combinations of 650 nm upper band probe (left column) and 740 nm lower band probe (right column) with lower band probe (lower row) and upper band probe (upper row). Probe wavelengths range from 720 nm to 740 nm in all images. Measurements 3201-3210, 3552-3561

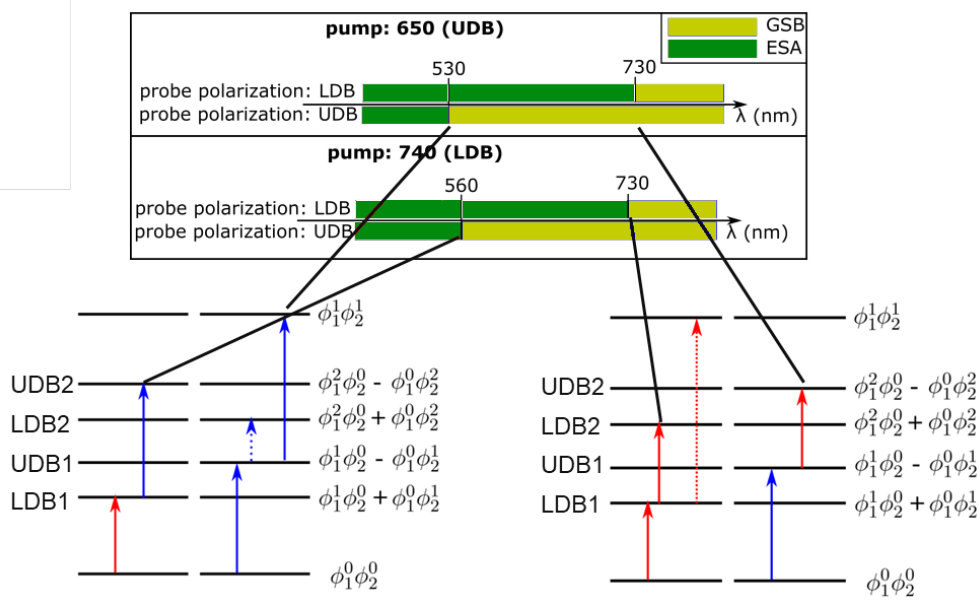


Figure 5.5.: Energy scheme of different combinations of excitations. GSB: ground state bleach, ESA: excited state absorption, UDB/LDB: upper/lower Davydov band, red arrow: lower band polarisation, blue arrow: upper band polarisation. Created by Pascal Heim, preliminary result.

5.1.1. 730 nm probe: Oscillations

It was first discovered that in measurements at 740 nm that were not reproducible, the exponentially decaying signal is superimposed with a decaying oscillation. However, as a sanity check, this set of measurements is performed at different delay step sizes to find if exterior influences such as nonlinear stage movement or variations in laser power result in these oscillations. The result is therefore verified by varying the step size.

Subsequent measurements show that this is true for many wavelengths with p_{LDB} probe polarization, but is most clearly visible at 730 nm as can be seen in figure 5.6. Reference [15] describes a similar behaviour in KTCNQ as coherent phonons oscillating along the stacking axis; however, up to the point of this thesis, it has not been shown that this mechanism is indeed the cause of oscillations in orthorombic SQIB. Extracting the oscillating signal is done by fitting a model function according to reference [9] (see also reference 3.5); then, the Fourier transformation is calculated from the entire remaining signal. Table 5.1 shows the corresponding fit constants for state population at 650 nm p_{UDB} pump and 730 nm p_{LDB} probe. It is noteworthy that this measurements includes a comparatively long decay at 350 ps; this may be associated with fluorescent emission or a dark decay, and very likely is the result of ground-state depletion. After the subtraction of four exponential decays, the remaining signal in figure 5.6c can be Fourier transformed to yield figure 5.6d, revealing an oscillation frequency of ≈ 1 THz.

Table 5.1.: Fit for 650 nm p_{UDB} pump, 730 nm p_{LDB} probe according to equation (3.11). σ is the edge steepness, τ_i decay constants. τ_1 is associated with the first peak and τ_4 with the longest decay beyond the range of the delay stage.

Component	Value
σ	0.118(1) ps
τ_1	0.023(1) ps
τ_2	6.7(1) ps
τ_3	5.8(1) ps
τ_4	350(20) ps

A second effect at 730 nm is that, after an initial peak associated with excited state absorption, there is a dip into the ground state depletion/stimulated emission region. This points towards a linear combination of these effects; as a matter of fact, a combination of 650 nm p_{UDB} pump/715 nm p_{LDB} probe and 650 nm UDB pump and 740 nm p_{LDB} probe yields the same shape as 650 nm p_{UDB} pump and 730 nm p_{LDB} probe as can be seen in figure 5.7. This is achieved with the following equation:

$$\Delta T_{\text{fit}}(730 \text{ nm}) = 1196 * \Delta T(715 \text{ nm}) + 667 * \Delta T(740 \text{ nm})$$

where both factors are derived from manual adjustment of peak heights. Fits according

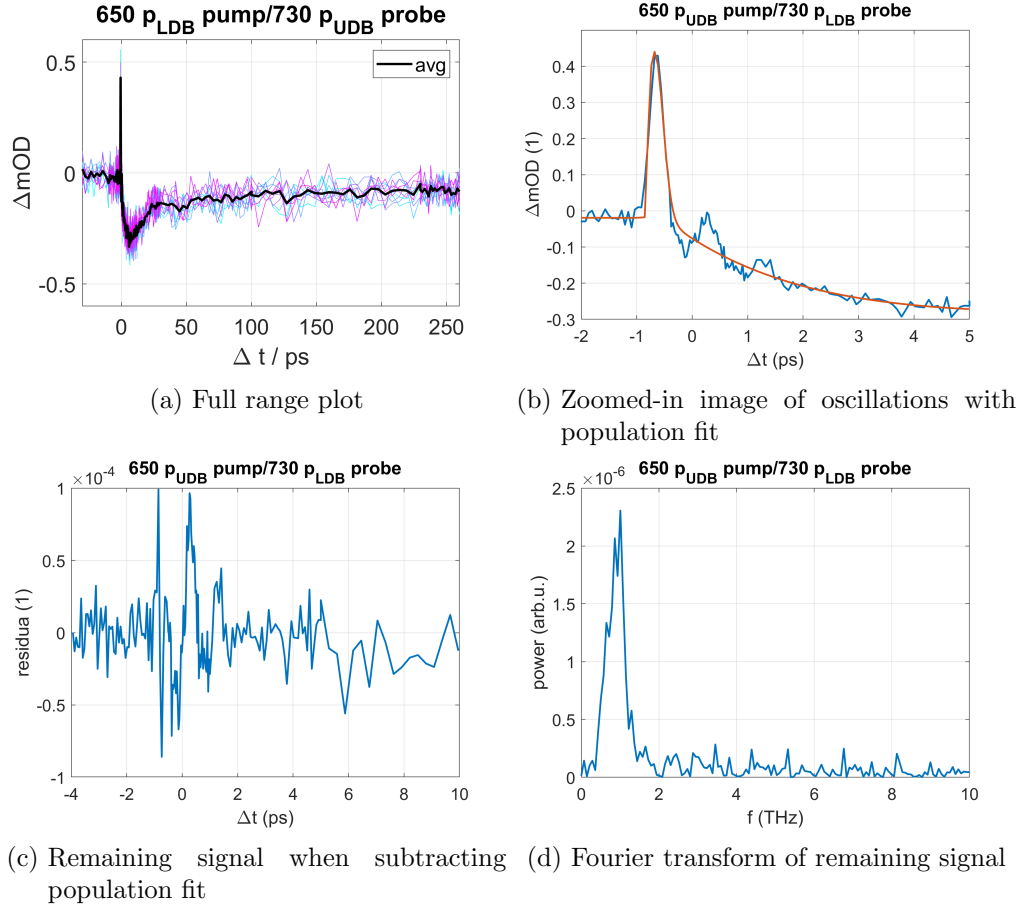


Figure 5.6.: Oscillations at 650 nm p_{UBD} pump, 730 nm p_{LDB} probe. This combination shows very strong oscillations with a period of ≈ 1 ps, but similar oscillations can also be seen at other LDB probe graphs. Measurement 3154-3163

to equation (3.11) yield decay constants of

- $\tau(715 \text{ nm}) = 4(1) \text{ ps}$ and $8(1) \text{ ps}$
- $\tau(730 \text{ nm}) = 0.03(1) \text{ ps}$, $6(1) \text{ ps}$, $8(1) \text{ ps}$ and $350(5) \text{ ps}$
- $\tau(740 \text{ nm}) = 7(1) \text{ ps}$ and $9(1) \text{ ps}$

Longer measurements would improve the signal-to-noise ratio and make the fit constants, as well as the number of exponential decays needed for correct fits, more exact.

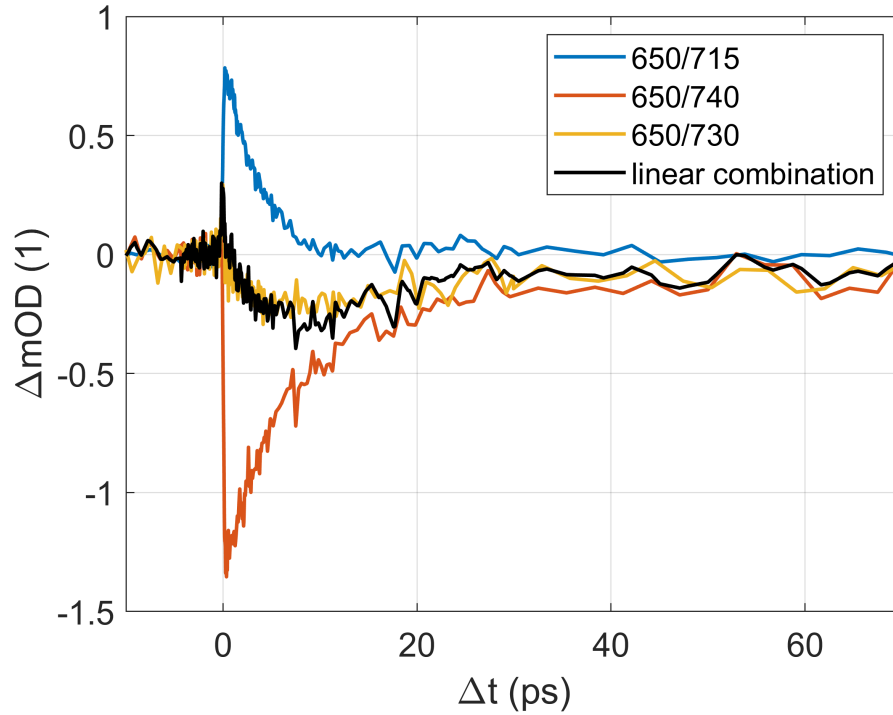


Figure 5.7.: Delay scans of 650 nm UDB pump with 715 nm, 730 nm and 740 nm LDB probe. The black line is a linear combination of 715 nm and 740 nm that has, within noise, the same shape as that of 730 nm probe. Measurements 3199, 3203, 3206.

5.2. Femtosecond Dynamics

5.2.1. Population transfer

Figure 5.8 shows the combination of 650 nm upper Davydov pump and 740 nm lower Davydov probe. Unfortunately, the measurement series shows a change in background intensity with measurement time, indicating some photodamage on the spot measured;

however, the shape of the curve stays the same throughout the series, indicating no chemical changes in the composition. The fit to equation (3.11) fits well with two exponentially decaying components at 2.7(3) ps and 10.4(3) ps. A possible explanation is:

1. A significant population of UDB1 is created by the pump pulse, but decays into LDB1 within ≈ 100 fs within the rising edge
2. From LDB1, this population can undergo stimulated emission by the 740 nm p_{LDB} probe pulse, but decays into intermediary states without emission with a decay constant of 2.7(3) ps
3. Ground state depletion can still be seen as the population decays back into the ground state at 10.4(3) ps

The upper image figure 5.8a also shows the absence of photodamage during the measurement series as the curves would change their shape in this case.

In case of figure 5.8, the UDB1 is pumped at 650 nm, close to its maximum absorption and the probe beam is also set to its maximum absorption at 740 nm resulting in efficient probing for the LDB state. It can be seen that ground state bleach, maybe including some stimulated emission, shows the largest effect at this combination of wavelength and polarization. The same is true for figure 5.9 with p_{UDB} polarizations at the same wavelengths, but with considerable less TA intensity (≈ 0.2 mOD compared to 1.4 mOD).

Figure 5.10 shows pumping and probing at 650 nm p_{LDB} and 740 nm p_{LDB} . What is surprising is that, in spite of less pump efficiency, this measurement is close to the transient intensity of the crossed polarizations (p_{UDB}/p_{LDB}).

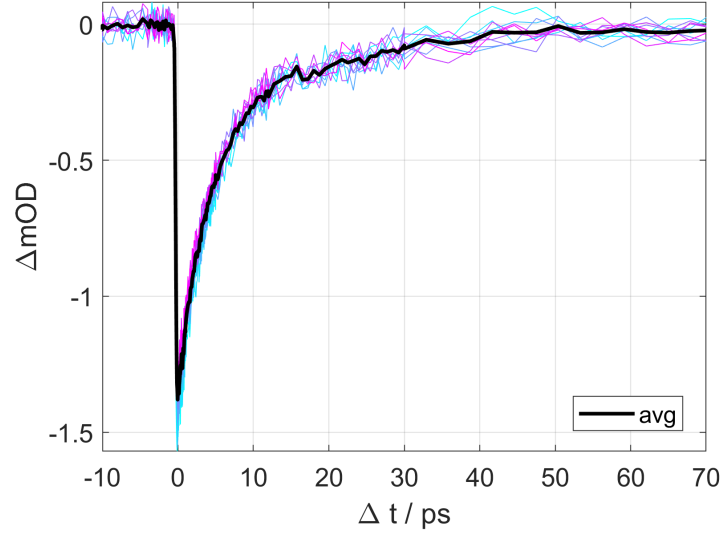
Figure 5.11 shows the case of pumping and probing at 740 nm p_{LDB} . Unlike other measurements, there seems to be only one exponentially decaying effect as the decay times almost match when selecting two distinct functions in addition to that covering the first peak.

Figure 5.12 shows a case where three decay constants are needed for a good fit to the experimental results. Which decay processes contribute to this is still up to discussion at the time of writing this thesis.

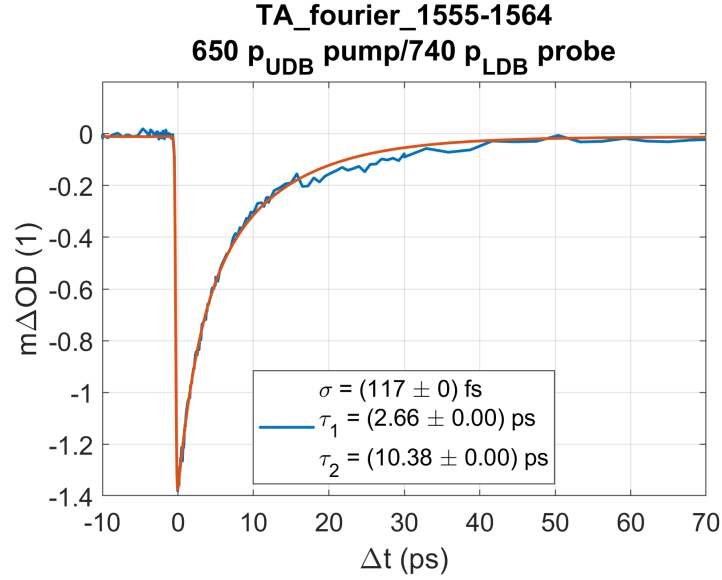
5.2.2. Polarisation scan at 450 nm probe

At 450 nm, excited state absorption is the dominant effect regardless of pump settings. One of the goals here is to determine whether the change in ESA transient absorbance depends on the polarisation of 450 nm probe light. As figure 5.13 indicates, there is indeed a polarisation dependency, albeit smaller than when probing the upper or lower bands directly. For this set of measurements, the Orpheus-N-2H is used as probe laser and frequency doubled with a 1 mm BBO crystal to achieve 450 nm of probe wavelength. The pump power is increased to 0.38 μ W (19 nJ per pulse) to increase the signal whereas the probe is kept at a standard 0.25 μ W (6.25 nJ per pulse). By fitting with

$$\Delta A(\alpha) = A_0 \sin(8\pi\alpha + \phi)$$



(a) Individual measurements (cyan to magenta) and average value (black). Stray light is removed by subtracting the average of the thirist 30 probe-pump values.



(b) Double-exponential fit and both decay constants.

Figure 5.8.: TA delay scan of 650 nm p_{UDB} pump, 740 nm p_{LDB} probe. From the changes in background radiation on the probe-pump side, slight deterioration of the sample might be present; however, the shape of all curves is very similar. Fit uncertainties in the legend are only based on fit estimates, mutiple measurement indicate $\tau_1 = 2.7(3)$ ps and $\tau_2 = 10.4(3)$ ps.

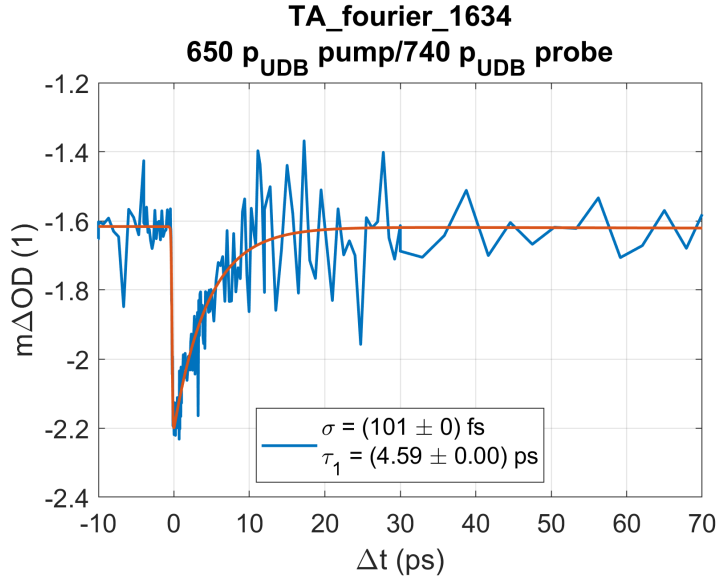


Figure 5.9.: TA delay scan of 650 nm p_{UBD} pump, 740 nm p_{UBD} probe. A single exponential fit results in 4.6(5) ps of decay time, measurement 1634. More measurements are needed to determine possible population transfer.

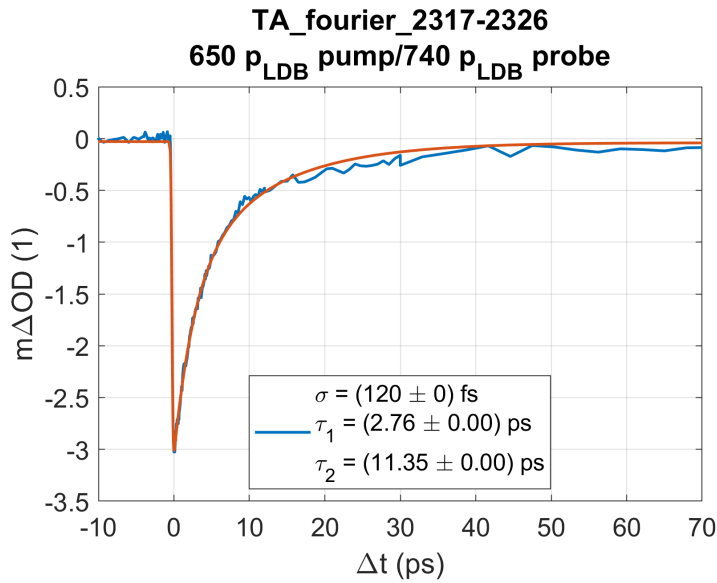


Figure 5.10.: TA delay scan of 650 nm p_{LDB} pump, 740 nm p_{LDB} probe. $\tau_1 = 2.8(1) \text{ ps}$, $\tau_2 = 11.5(5) \text{ ps}$, measurements 2317-2326.

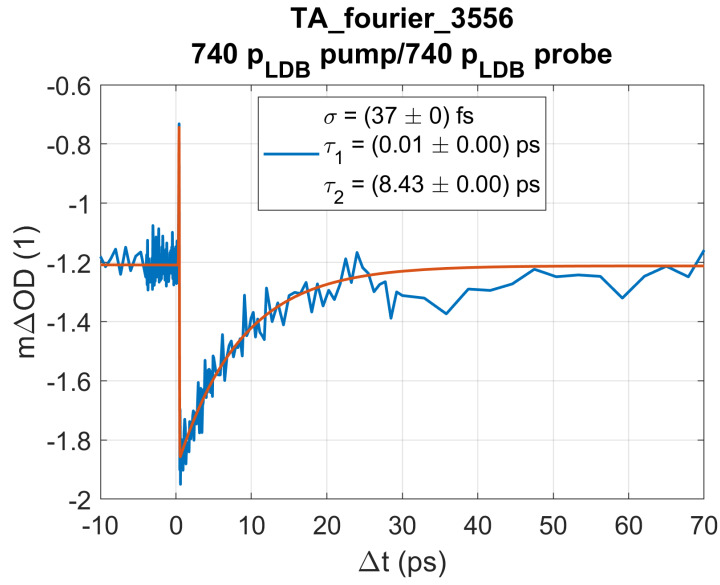


Figure 5.11.: TA delay scan of 740 nm p_{LDB} pump and probe. Single decay time $\tau_2 = 8(1) \text{ ps}$ (uncertainty based on varied starting conditions for fit), measurement 3556. τ_1 results from the first peak only.

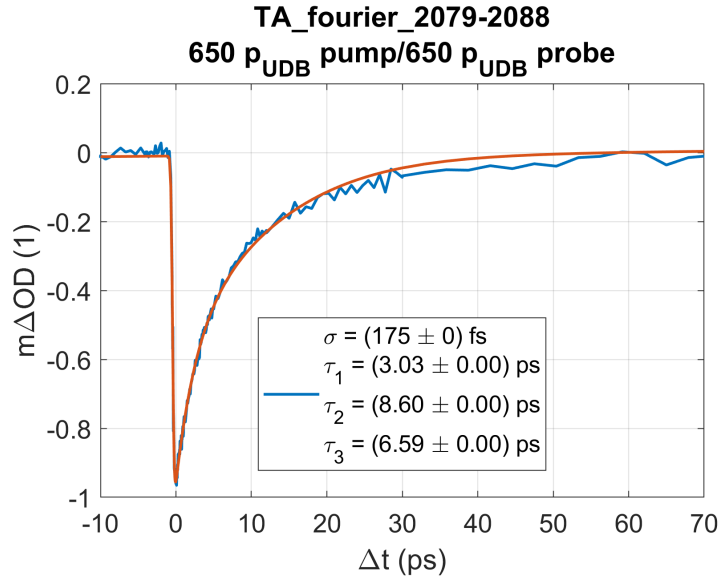


Figure 5.12.: Triple-exponential fit of 650 nm UDB pump and probe. Decay times $\tau_1 = 3.0(3) \text{ ps}$, $\tau_2 = 6.6(5) \text{ ps}$, $\tau_3 = 8.6(5) \text{ ps}$ based on binned measurements, measurements 2079-2088.

taking into account the \sin^2 behaviour of polarisations and the 2α change in polarisation caused by the $\lambda/2$ plate. According to the fit, the transient absorbance changes by a maximum of 38 % at upper band pump and 39 % at the lower band pump. In figure 5.13, the positions of minimum single-pulse transmission could theoretically be added based on the same measurement; however, this data showed no oscillating behaviour which can be attributed to sample degradation, preventing the possibility of a useful sinusoidal fit.

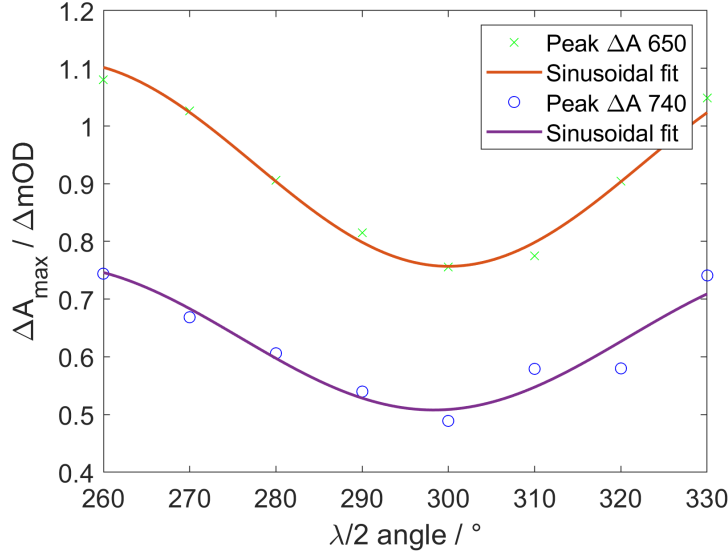


Figure 5.13.: Polarisation dependency of excited state absorption peak transient absorbance at 650 nm p_{UDB} pump and 740 nm p_{LDB} pump, each with 450 nm p_{UDB} probe. Measurements Polarization_TA_Scan.0000 and 0001.

5.3. Transient Absorption Imaging

The main purpose of using a TA microscope for SQIB samples is the ability to perform transient absorption measurements at specific points on the sample without averaging over more than one platelet; the fast scanning capability of the xy stage is not very important for purposes of this master thesis. However, there are some exceptions.

Homogeneity of platelet orientation Figure 5.14 shows the homogeneity of transient absorption images within a domain. SQIB sample 6 was glued to another microscope slide with its thin film side inside an inert argon atmosphere in an attempt to reduce the amount of photodamage; however, the center of the images clearly shows that it can still happen. For this set of scans, a pump power of $0.90(2) \mu\text{W}$ and a probe power of $1.20(2) \mu\text{W}$ before the first objective were chosen, much higher than the $0.25 \mu\text{W}$ used by default for crystalline SQIB samples when more experience was made with deterioration.

Multiple platelets, ground state depletion Figure 5.15, by contrast, shows the influence of different domain orientations by extending the scan range on SQIB sample 3. For this measurement, standard powers were used for pumping the upper Davydov band and probing the lower band. At this combination of 650 nm UDB pump, 740 nm LDB probe (as set up in the center of this image), there is mainly a difference in TA contrast for different SQIB orientations while ground state depletion or stimulated emission effects dominate in the whole scan range. This is a good indication for the absence of higher excitations for this combination of wavelengths as they would show as excited state absorption, resulting in a positive change in absorbance after the pump-probe overlap.

Multiple platelets, ground state depletion and excited state absorption Figure 5.16 shows clearly how the choice of polarisation affects which states can be excited as, at the same wavelength, there are parts of the sample mainly exhibiting excited state absorption while the rest is dominated by ground state depletion and/or stimulated emission. Transmission images of the same region at 650 nm also show the different orientations in the platelets under investigation.

Spikes In several experimental conditions, there are spikes in the TA signal close to the temporal overlap. While the reason is not known as of this Master thesis, it is worthwhile to check if this effect happens across a larger region and if, upon repeated measurement, the direction of the signal remains the same. Figure 5.17 is a measurement of the first kind: At 740 nm upper Davydov pump and 730 nm lower Davydov probe, there is a strong peak directly after the overlap.

Zero-crossing One set of images is recorded at 650 nm p_{UDB} pump and 730 nm p_{LDB} probe similar to the results in section 5.1.1. This image shows that the superposition of excited state absorption with its long decay constant and the quicker ground state bleach/stimulated emission happens within the whole domain scanned, albeit with different intensities.

2D fitting Using a long series of transient absorption images taken at different decays, it is possible to determine the transient absorbance amplitude, as well as the first decay constant for each pixel individually. Such a measurement is shown in figure 5.19. It can be seen that, for this combination of wavelengths and polarisations, domain boundaries are clearly visible only in the amplitude relating to the orientation of the crystal lattice, not in the decay constant.

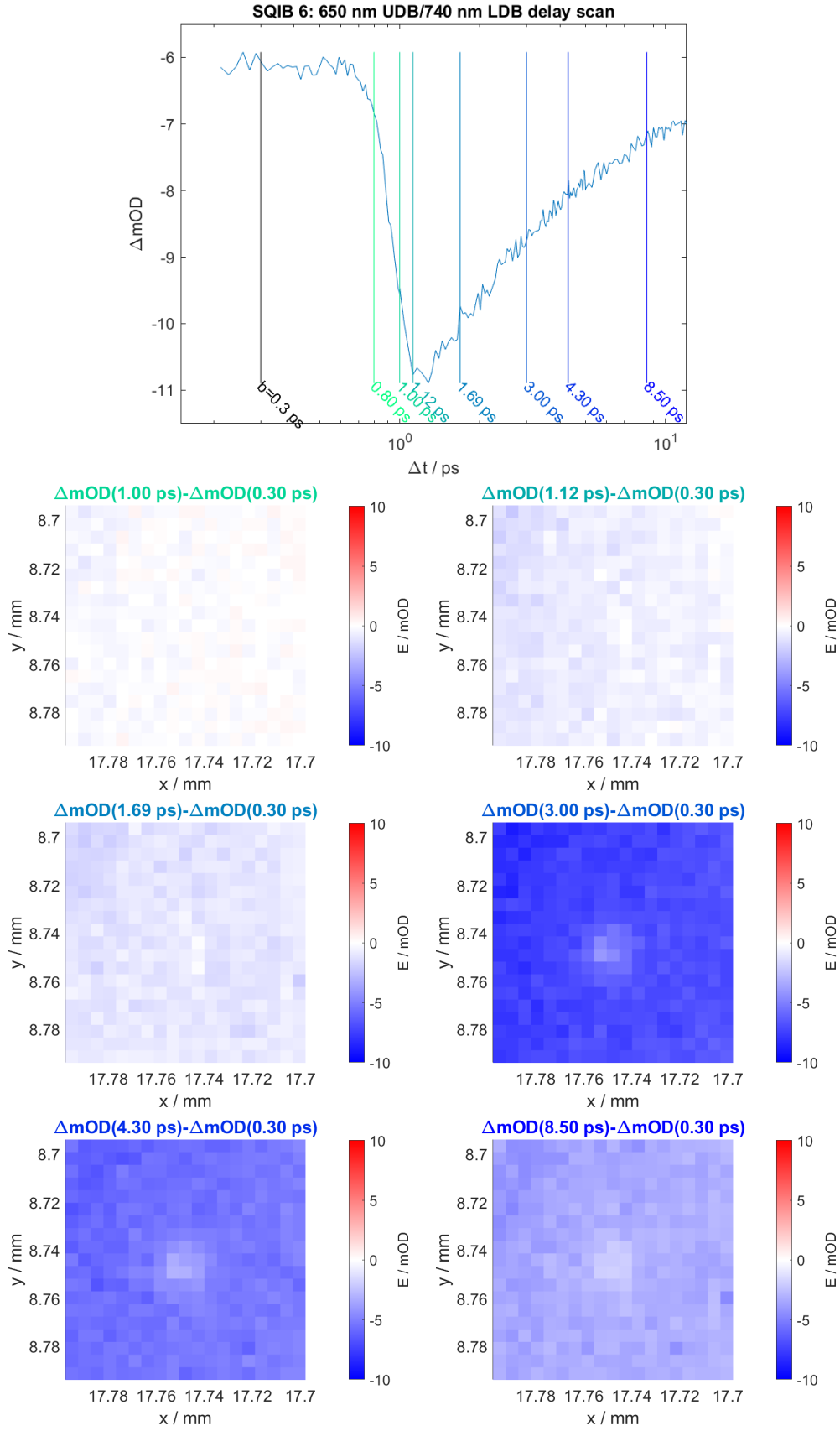


Figure 5.14.: Image scan within a domain on SQIB sample 6 (orthorhombic SQIB encased between glass plates in an inert Argon atmosphere). The central spot is deterioration from long laser exposure. $b = 0.3 ps$ in the delay scan denotes the baseline subtracted from all other images. There is a shift between the delay scan and the times indicated. Images 0043-0050, delay scan 0467

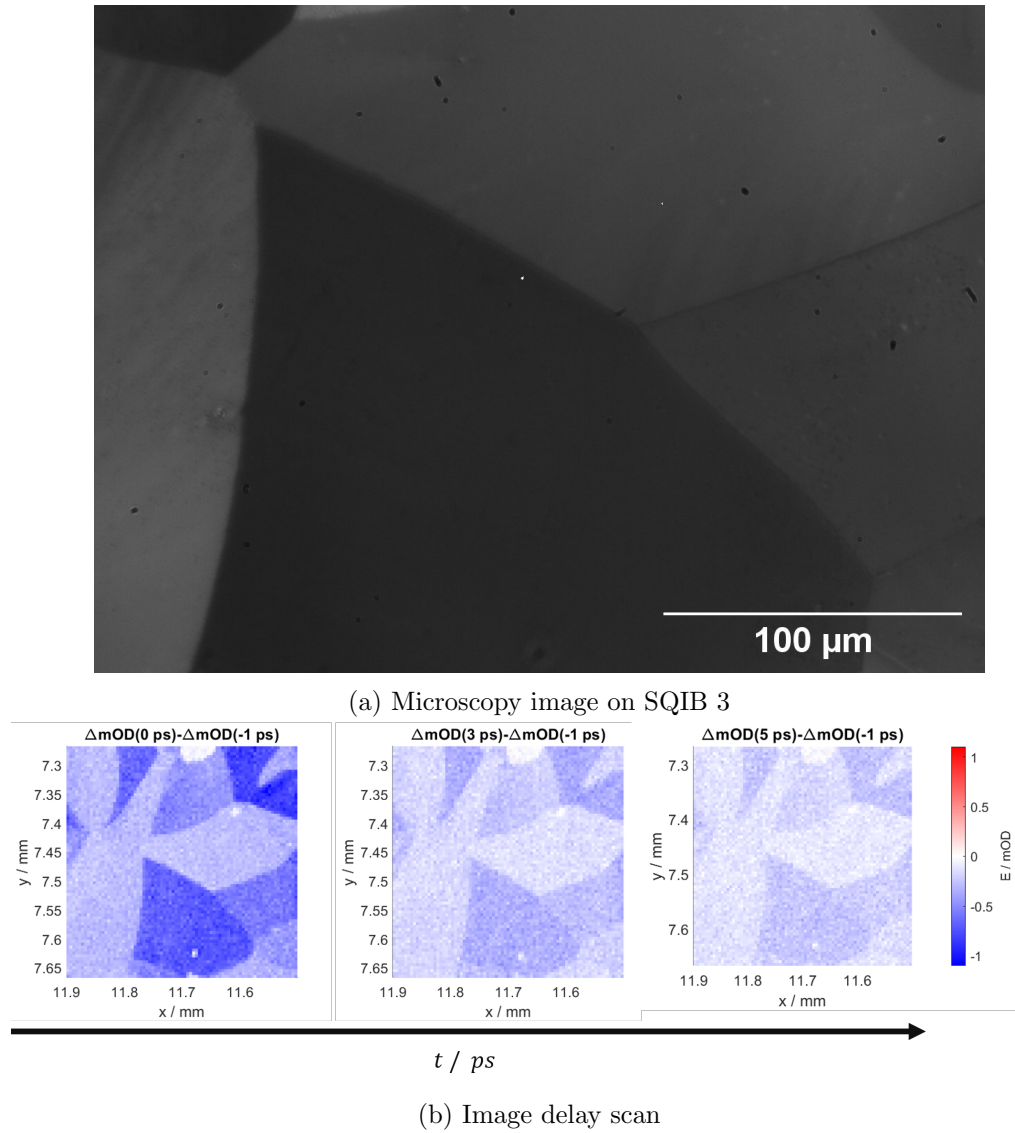


Figure 5.15.: Different domain orientations visualised by a transient absorption image at 650 nm UDB pump, 740 nm LDB probe (polarisation is set up at the center of this image). The upper image shows the central region of the TA scans as seen through crossed polarisers in transmission microscopy. Images 0133-0141

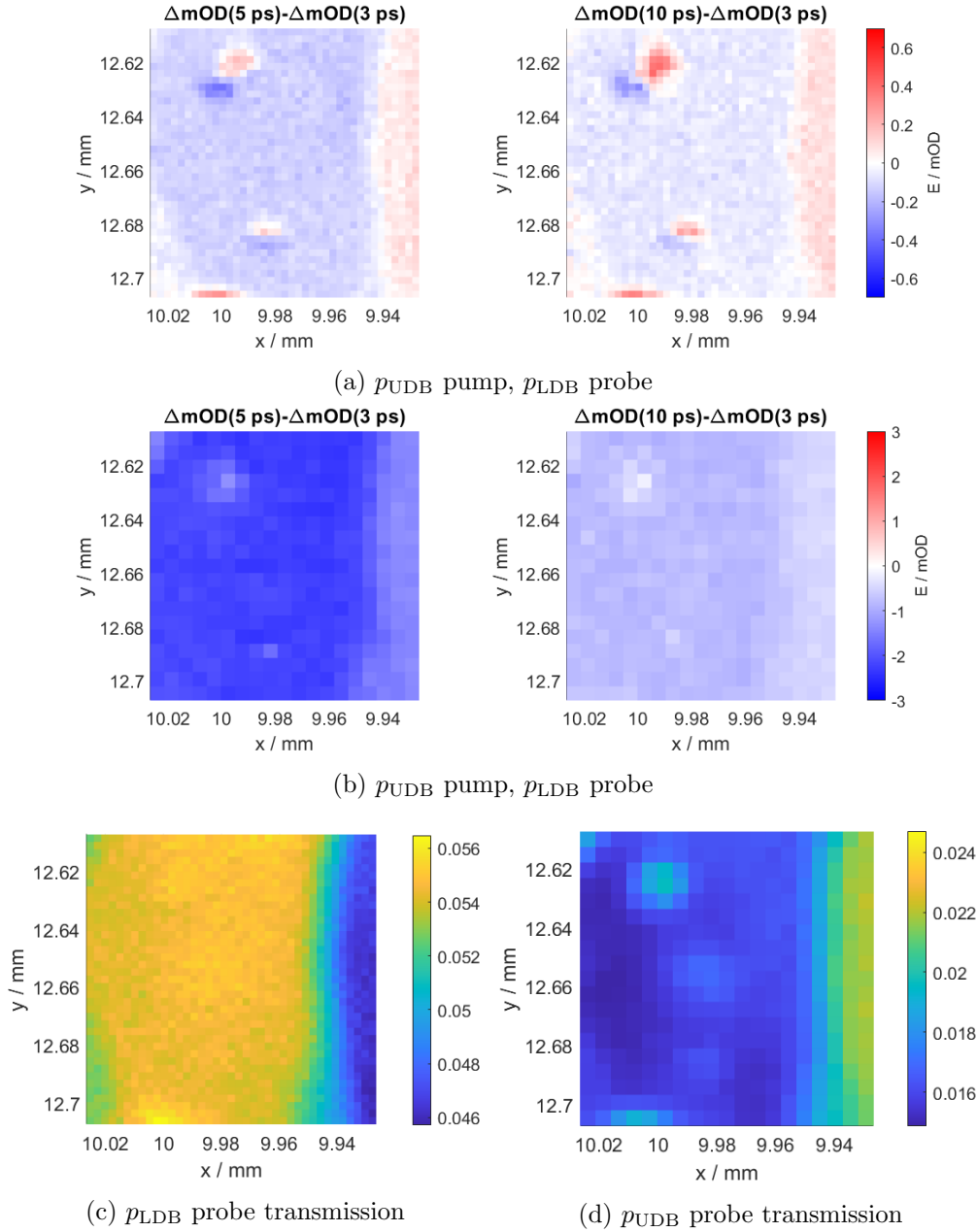


Figure 5.16.: 650 nm p_{UBD} pump, 650 nm p_{UBD} probe images on the same platelets on SQIB 3. a is an example for different behaviour across platelet boundaries: The region on the right is similar to upper pump, lower probe measurements with excited state absorption dominating. Differently looking spots are likely due to deterioration or imperfections of the sample. The signal at 3 ps corresponds to probe-pump background and is subtracted from the corresponding images. For reference, a wrong-color image of the probe intensity is added for both polarisations at 650 nm. Images 0152-0157

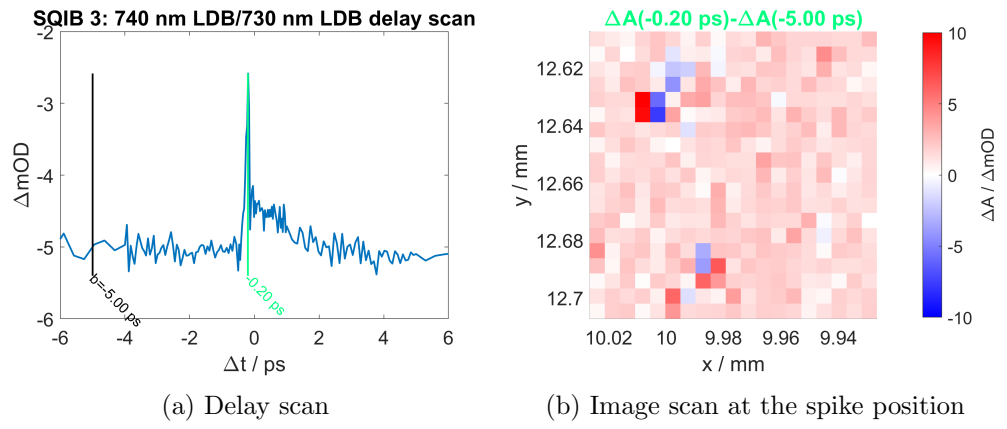


Figure 5.17.: Delay scan and image of the spike position at 740 nm lower Davydov pump, 730 nm lower Davydov probe. b denotes the position whose background intensity is subtracted, $\Delta E = 0.1$ mOD.

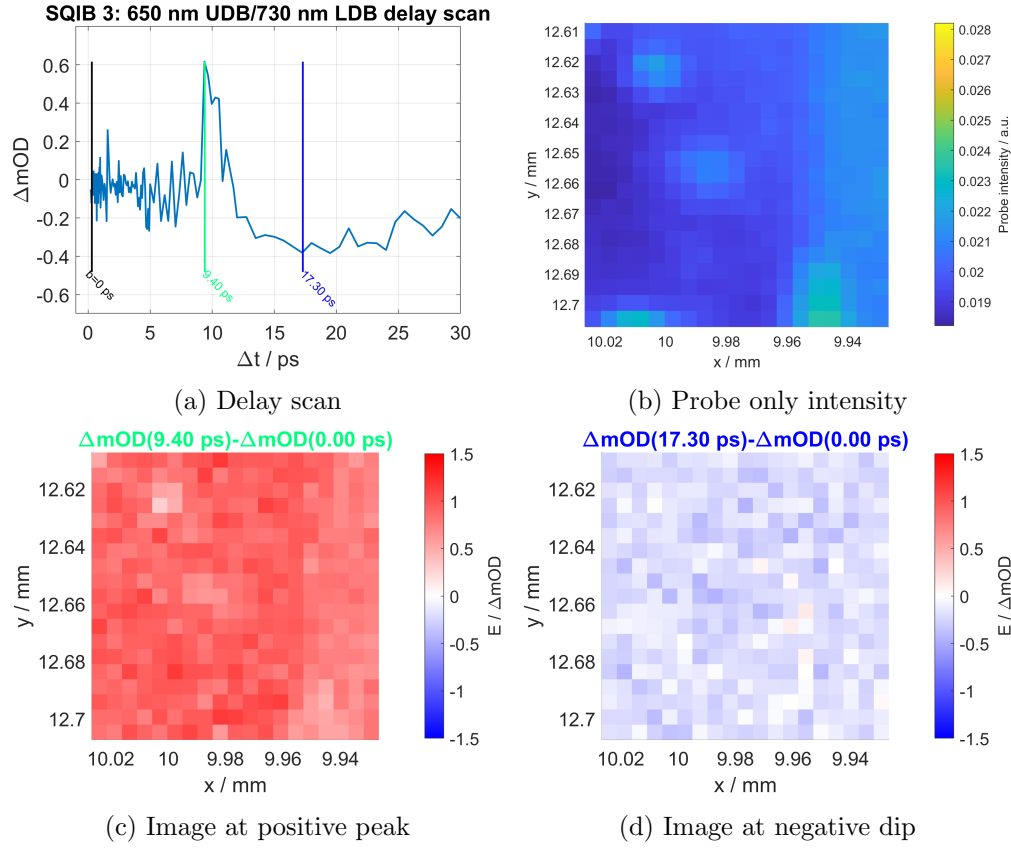


Figure 5.18.: Delay scan and images at positive and negative peaks in the transient absorption curve at 650 nm upper pump, 740 nm lower probe of SQIB sample 3. $\Delta E = 0.1 \text{ mOD}$. The region to the right of c is likely a neighbouring platelet with a slightly different orientation as the probe only transmission is different there.

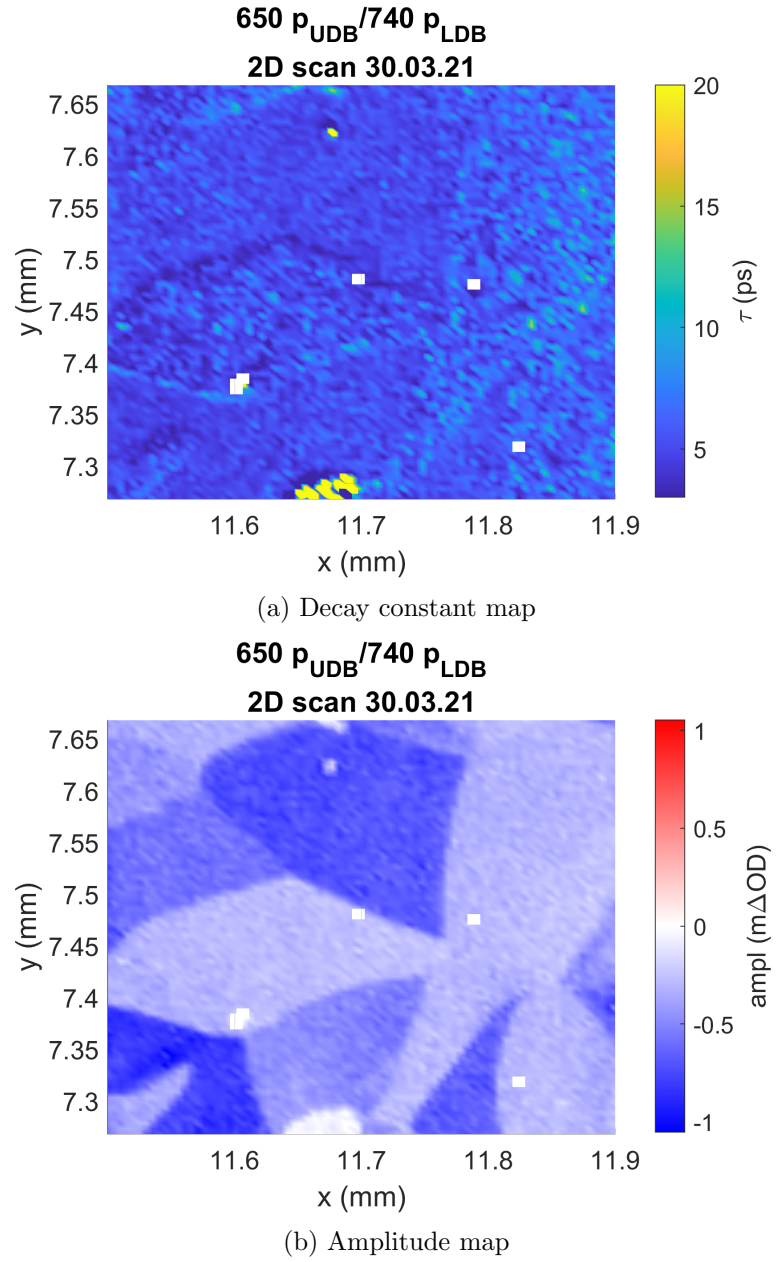
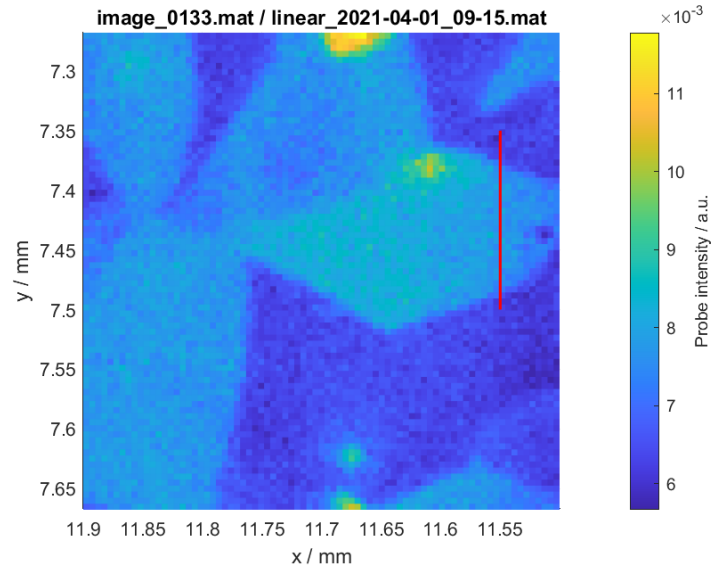


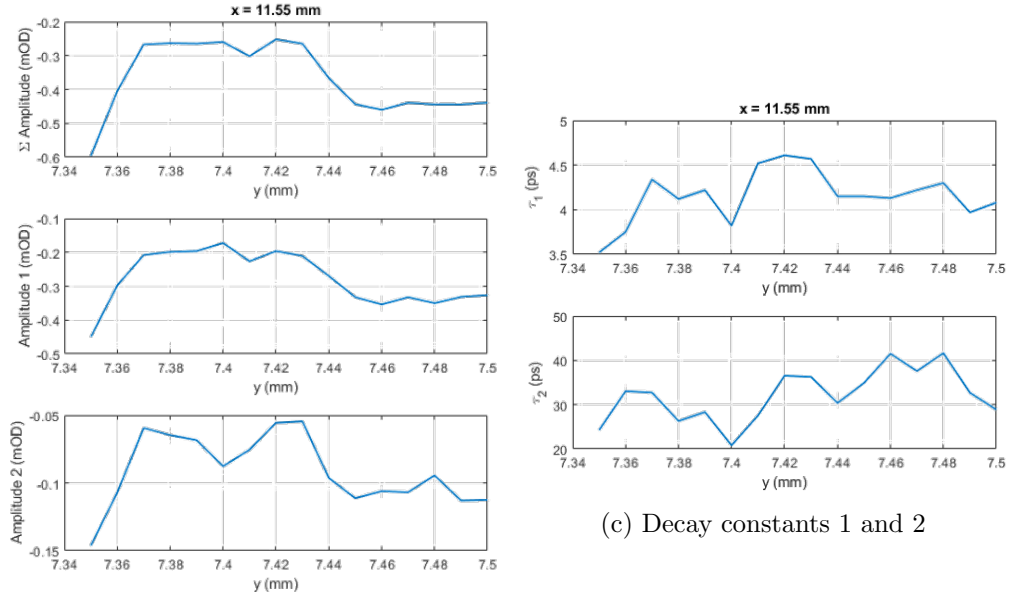
Figure 5.19.: 2D transient absorption fit across multiple platelets on orthorhombic SQIB 3. Using colormap [1] for plotting the results of images 133-141 and series 2021-03-30_08-48, 2021-03-30_19-26 and 2021-03-31_07-16.

5.4. Linear delay scan series

Figure 5.20 shows a set of delay scans taken at equally spaced points along a line as indicated in the transmission image. The goal here was to see how much the maximum amplitude in transient absorbance and the delay constants change within a platelet and when crossing its boundaries. It can be clearly seen that the domain boundaries do not have a noticeable influence on the decay times, but a strong influence on the amplitude. Also, there is considerable variation in both fit parameters within a single domain (fitting errors are usually much less than 1 %.)



(a) Scan region transmission with linear scan highlighted in red



(b) Amplitudes (sum, decay 1, decay 2)

(c) Decay constants 1 and 2

Figure 5.20.: Fitting constants of delay scans along a line crossing a platelet boundary. This was done to determine if platelet boundaries are noticeable in fitting constants; it can be seen that this is indeed the case for transient absorbance intensity, but not in the exponential decay constants. Settings: 650 nm p_{UDB} pump, 740 nm p_{LDB} probe at the start of the linear scan.

6. Outlook

6.1. Ultrafast exciton dynamics

While the work on measurements on orthorhombic SQIB on the transient absorption microscope is likely done, the Koch group at TU Graz expects to gain more insight into the processes governing the exciton excitations inside the molecular crystal. As of writing this thesis, there is a basic understanding of higher excited states that can only be examined with ultrafast lasers due to the short lifetime of single excited states. However, the dynamics themselves are still under investigation: Is there a population transfer between upper and lower Davydov bands? How quickly does it happen? For further research, Frank T. Spano from University of Temple has been contacted to provide additional insight into crystalline SQIB.

6.2. Oscillations

Moreover, the oscillations explained in section 5.1.1 that appear when probing the lower Davydov band around 730 nm are yet to be understood fully. While the curve is in close resemblance to coherent phonons explained in reference [15], research has to be undertaken to describe the exact phenomenon and rule out other effects such as vibronic transitions. This can probably be done by investigating SQIB outside of its crystalline form, for example dissolved in a thin film of PMMA (poly-(methyl methacrylate)) or in its pure, non-crystallised form. These experiments are performed by Leo Felix Angermann, also within the Koch group.

6.3. Setup

Considering the transient absorption microscopy itself, there are some improvements that can enhance further measurements:

- Higher NA objectives to achieve a higher spacial resolution
- Actuated $\lambda/2$ plates to automate polarisation scans
- Wavelength change automation, necessitating a power feedback and automated neutral density filters due to the power dependency on wavelength in NOPAs
- More optimisation of the integrated prism compressors to achieve pulses as short as possible (this was not deemed necessary for the phenomena under investigation yet)

A. List of Devices

Table A.1.: List of devices used

Title	Remarks
Light Conversion PHAROS	Yb:KGW femtosecond laser, PH1-20-0400-02-30, L191103; 40 kHz repetition rate at 400 μ J pulse energy
Light Conversion ORPHEUS N-3H	NOPA, $\lambda = 500$ nm to 950 nm
Light Conversion ORPHEUS N-2H	NOPA, $\lambda = 640$ nm to 950 nm
Scitec 310 CD with 300CD200HS	Optical chopper, frequency ≈ 1000 Hz to 55 000 Hz, focusing on chopper wheel using two $f = 125$ mm plano-convex N-BK7 lenses
Scitec S310Sync synchroniser	Phase and frequency locking of the chopper to external sources (function generator, laser sync output, frequency divider)
Thorlabs AHWP05M-600	400 nm to 800 nm achromatic $\frac{\lambda}{2}$ plate
Thorlabs AHWP10M-980	690 nm to 1200 nm achromatic $\frac{\lambda}{2}$ plate
Thorlabs NExxA series, Thorlabs NDxxA series, Eksma Optics 240-25xx series	Reflective and absorptive neutral density filters, used for coarse power setting
Reflective variable neutral density filters	Used to set input power exactly
OG530, RG715, RG780, RG830, RG850	Color glass filters
Thorlabs FESH0700, Newport FS-SWF set	Sputtered short-pass filters
Thorlabs FELH0700	Sputtered long-pass filter
Thorlabs WP25M-UB	Ultra-broad wire grid polariser
Film polarisers	For visible imaging microscopy

Continued on next page

A. List of Devices

Title	Remarks
Olympus UPlan FL N 10x	Focussing objective, 10x magnification, NA=0.3
Nikon Plan 10/0.3 160/0.17	Imaging objective, 10x magnification, NA=0.3
Lincoln HighLED White	For visible imaging microscopy
The Imaging Source DMK 42AUC03	Monochrome camera, particularly for spatial overlap alignment, beam shape characterization and orientation on the sample
Prototype, PHD1C_1 and PHD1C_2	High-speed optical detectors based on Hamamatsu S1336-8BK photodiode, JFET operational amplifiers, an analogue long-pass filter for signal elongation and impedance converters for calibration
Picoscope 5000 series	Oscilloscope used for data collection from optical detectors
Coherent LabMax Pro	Pulse measuring head, used for optimizing OPA output find exact specs
Coherent FieldMate with OP2-VIS measuring head	Laser power meter, used for setting input power
Newport LTA-HS	Delay stage actuator
Thorlabs Z825B, KDC101	Microscopy sample stage actuators (horizontal and vertical)
Various aluminium mirrors	Planar and concave (for focussing onto detectors)
74HC73	Dual JK flip-flop for frequency division

B. List of Figures

1.1. Principle of transient absorption microscopy	13
1.2. Contrast mechanisms in transient absorption	15
2.1. Setup of the transient absorption microscope	18
2.2. Determination of the resolution limit of the TAM setup.	20
2.3. Cross-correlation measurement for determining the temporal resolution at the sample	21
2.4. Sound spectra of the chopper recorded with a smartphone running Spec- troid from ≈ 1 m distance. Red: Maximum volume. Yellow: Current volume.	23
2.5. Setup for the calibration of the chopper synchroniser	24
2.6. Phase between reference signal and laser intensity on the photodiode when calibrating the chopper	25
2.7. Frequently used spectra for measurements	28
2.8. Spatially separated pump probe calibration setup	29
2.9. Setup for calibrating the motorized mirror mount	31
3.1. Comparison between interference filtering and mechanical filtering	34
3.2. Scan modes of the transient absorption microscope	36
3.3. liveFit interface	39
4.1. Energy scheme of Davydov splitting in case of dimers	41
4.2. SQIB molecular structure	42
4.3. Absorbance of an orthorhombic SQIB platelet recorded with a single po- lariser	44
4.4. Various images of spots on the sample SQIB 3 (orthorhombic SQIB ex- posed to ambient condition) between crossed polarisers	45
4.5. Spot degradation on SQIB sample 6. As the domains act similarly to a polarisation filter, microscope images recorded with the sample being between crossed polarisers show either lighter or darker spots depending on the orientation of the polarisers as in a. b shows a significant elongation in decay time with the time elapsed during the laser exposure. c includes a delay scan of a central, photodamaged spot in comparison to delay scans directly adjacent within the same domain, including a complete change in transient absorption effects.	47
5.1. Energy scheme of single and double excitations in SQIB	49

5.2. Zero-crossing point from ground state depletion/stimulated emission to excited state absorption for 650 nm p_{UDB} pump and varied upper band probe wavelength	51
5.3. Zero-crossing point from ground state depletion/stimulated emission to excited state absorption for 650 nm p_{UDB} pump and varied p_{UDB} probe wavelength	52
5.4. Combinations of 650 nm upper band probe (left column) and 740 nm lower band probe (right column) with lower band probe (lower row) and upper band probe (upper row). Probe wavelengths range from 720 nm to 740 nm in all images. Measurements 3201-3210, 3552-3561	54
5.5. Energy scheme of different combinations of excitations	55
5.6. Oscillations at 650 nm p_{UDB} pump, 730 nm p_{LDB} probe	57
5.7. Delay scans of 650 nm UDB pump with 715 nm, 730 nm and 740 nm LDB probe	58
5.8. TA delay scan of 650 nm UDB pump, 740 nm LDB probe	60
5.9. TA delay scan of 650 nm UDB pump, 740 nm UDB probe	61
5.10. TA delay scan of 650 nm p_{LDB} pump, 740 nm p_{LDB} probe. $\tau_1 = 2.8(1)$ ps, $\tau_2 = 11.5(5)$ ps, measurements 2317-2326.	61
5.11. TA delay scan of 740 nm p_{LDB} pump and probe	62
5.12. Triple-exponential fit of 650 nm UDB pump and probe. Decay times $\tau_1 = 3.0(3)$ ps, $\tau_2 = 6.6(5)$ ps, $\tau_3 = 8.6(5)$ ps based on binned measurements, measurements 2079-2088.	62
5.13. Polarisation dependency of excited state absorption peak transient absorbance at 650 nm upper pump and 740 nm lower pump, each with 450 nm upper probe.	63
5.14. Image scan within a domain on encased SQIB sample 6	65
5.15. Different domain orientations visualised by a transient absorption image	66
5.16. 650 nm p_{UDB} pump and probe transient absorption images on SQIB 3	67
5.17. Delay scan and image of the spike position at 740 nm lower Davydov pump, 730 nm lower Davydov probe	68
5.18. Delay scan and images at positive and negative peaks in the transient absorption curve at 650 nm upper pump, 740 nm lower probe of SQIB sample 3	69
5.19. 2D transient absorption fit across multiple platelets on orthorhombic SQIB 3	70
5.20. Fitting constants of delay scans along a line crossing a platelet boundary	72

C. List of Tables

2.1. Positive half cycle duration and total chopping duration at different frequencies	26
2.2. Calibration factors for the motorized mirror mount	30
5.1. Fit constants for 650 nm p_{UDB} pump, 730 nm p_{LDB} probe	56
A.1. List of devices used	75

Bibliography

- [1] Adam Auton. *Red Blue Colormap*. 2021. URL: <https://www.mathworks.com/matlabcentral/fileexchange/25536-red-blue-colormap>.
- [2] Frank Balzer et al. “Spotlight on excitonic coupling in polymorphic and textured anilino squaraine thin films”. In: *Crystal Growth and Design* 17.12 (Dec. 2017). DOI: 10.1021/acs.cgd.7b01131.
- [3] Pu-Ting Dong and Ji-Xin Cheng. *Pump-probe microscopy: theory, instrumentation, and applications*. Tech. rep. 2017, 32(4).
- [4] “Electronic Excited States, Excitons, Energy Transfer”. In: *Organic Molecular Solids*. John Wiley & Sons, Ltd, 2006. Chap. 6. ISBN: 9783527618651. DOI: <https://doi.org/10.1002/9783527618651.ch6>.
- [5] Alexander Franzen. *ComponentLibrary*. URL: <http://www.gwoptics.org/ComponentLibrary/> (visited on 15/09/2021).
- [6] Michelle M. Gabriel et al. “Direct Imaging of Free Carrier and Trap Carrier Motion in Silicon Nanowires by Spatially-Separated Femtosecond Pump-Probe Microscopy”. In: *Nano Letters* 13.3 (Mar. 2013). DOI: 10.1021/nl400265b.
- [7] Erik M. Grumstrup et al. “Ultrafast Carrier Dynamics in Individual Silicon Nanowires: Characterization of Diameter-Dependent Carrier Lifetime and Surface Recombination with Pump-Probe Microscopy”. In: *The Journal of Physical Chemistry C* 118.16 (Apr. 2014). DOI: 10.1021/jp502737e.
- [8] Zhi Guo et al. “Spatial and temporal imaging of long-range charge transport in perovskite thin films by ultrafast microscopy”. In: *Nature Communications* 6.1 (Nov. 2015). DOI: 10.1038/ncomms8471.
- [9] Pascal Heim. “Analysis of molecular Rydberg state relaxation dynamics applying Bayesian probability theory”. Master. Graz University of Technology, 2017.
- [10] Pascal Heim. “Femtosecond Light-Matter Interaction Processes from Isolated Molecules to Molecular Crystals”. PhD thesis. 2021.
- [11] Heinz Köhler, Anna; Bäessler. “Electronic Processes in Organic Semiconductors”. In: John Wiley & Sons, Ltd, 2015. Chap. 1. ISBN: 9783527685172. DOI: <https://doi.org/10.1002/9783527685172.ch1>.
- [12] Eric S Massaro, Andrew H Hill and Erik M Grumstrup. “Super-Resolution Structured Pump-Probe Microscopy”. In: *ACS Photonics* 3.4 (2016). DOI: 10.1021/acsp Photonics.6b00140.

- [13] “Molecular and Lattice Dynamics in Organic Molecular Crystals”. In: *Organic Molecular Solids*. John Wiley & Sons, Ltd, 2006. Chap. 5. ISBN: 9783527618651. DOI: <https://doi.org/10.1002/9783527618651.ch5>.
- [14] Gero Nootz. *Fit 2D gaussian function to data*. 2012. URL: <https://de.mathworks.com/matlabcentral/fileexchange/37087-fit-2d-gaussian-function-to-data>.
- [15] Christopher C. Rich and Renee R. Frontiera. “Uncovering the Functional Role of Coherent Phonons during the Photoinduced Phase Transition in a Molecular Crystal”. In: *Journal of Physical Chemistry Letters* 11.18 (Sept. 2020). DOI: 10.1021/acs.jpclett.0c01834.
- [16] Markus Schwoerer and Hans Christoph Wolf. *Organic Molecular Solids*. 1st ed. Berlin: Wiley-VCH, 2006. ISBN: 978-3-527-40540-4.
- [17] Yifan Zhu and Ji Xin Cheng. *Transient absorption microscopy: Technological innovations and applications in materials science and life science*. Jan. 2020. DOI: 10.1063/1.5129123.